THE PENNSYLVANIA STATE UNIVERSITY
SCHREYER HONORS COLLEGE

DEPARTMENT OF ELECTRICAL ENGINEERING

EFFICIENT CORONA MODELS IN SPHERICAL GEOMETRY FOR LIGHTNING PROTECTION APPLICATIONS

ELIZABETH J. KOWALSKI
Spring 2008

A thesis
submitted in partial fulfillment
of the requirements
for a baccalaureate degree
in Electrical Engineering
with honors in Electrical Engineering

Reviewed and approved* by the following:

Victor P. Pasko
Associate Professor of Electrical Engineering
Thesis Supervisor

Sven G. Bilén
Associate Professor of Electrical Engineering
Honors Advisor

*Signatures are on file in the Schreyer Honors College.

Abstract

One-dimensional, spherical models for streamer corona have been developed to investigate the effects of a lightning rod's radius on the time of leader initiation. In the development of the final model, a numerical solution for the currrent–voltage relationship of stationary corona with spherically dependent charge density has been found. An analytical, closed form solution of this problem is not known [e.g., *Roth*, 1995, p. 253–255], and the related solution represents one of the original contributions of this thesis. The non-stationary corona model presented in this thesis is an improvement on the recent work by *Bazelyan et al.* [2008, and references within]. The non-stationary corona and upward leader model developed in this thesis numerically calculates the development of corona in a 1–D spherical system and accounts for streamer busts and upward leader initiation. The non-stationary model has been validated through comparison with the stationary solution, previous models [e.g., *Aleksandrov et al.*, 2002, *Bazelyan et al.*, 2008], and field data [*Moore et al.*, 2003]. The pulsing nature of the streamer bursts inhibits the formation of a leader and has been used to find an upper limit on the optimum lightning rod tip radius. Any optimum rod radii found should be less than 5 cm, and will likely be between 0–2 cm. However, no lower limit for the optimum rod radius can be set at this time. Further investigation into shielding effects may be able to provide additional constraints for the optimum lightning rod radii.

Table of Contents

List of Figures

List of Symbols

Δr	Discretization step in r-direction (m)
Δt	Discretization step in time (s)
ΔU_{st}	The voltage drop along the length of the streamer zone (V)
ε_0	Permittivity of free space ($\varepsilon_0 = 8.85 \times 10^{-12}$ F/m)
ε	Allowed error for non-stationary model bisection process (%)
μ_e	Electron mobility in air ($\text{m}^2/\text{V} \cdot \text{s}$)
μ_i	Ion mobility ($\mu_i = 1.5 \times 10^{-4}$ $\text{m}^2/\text{V} \cdot \text{s}$)
ν_a	Two-body dissociative attachment frequency (m^3/s)
ν_i	Ionization frequency (m^3/s)
ρ	Charge density (C/m^3)
τ	Non-stationary voltage rise-time (s)
E_c	Critical electric field for corona initiation ($E_c = 4.3 \times 10^6$ V/m)
E_0	Ambient electric field (V/m)
I_{ss}	Steady-state current for the non-stationary model (A)
q_e	Charge of an electron ($q_e = -1.61 \times 10^{-19}$ C)
R_1	Lightning rod tip radius/inner electrode radius (m)
R_2	Outer electrode radius (m)
t_c	Time of corona initiation (s)
t_L	Time of leader initiation (s)

t_{st} Time of first streamer corona initiation (s)

U_c Critical voltage for corona initiation (V)

U_0 Stationary voltage (V)

Acknowledgments

Without the dedicated help of Mr. Jérémy Riousset and Dr. Victor P. Pasko this thesis would not have happened. I must express my gratitude to them for introducing me to the subject matter and helping me complete this research. I must also thank Dr. Sven Bilén, my honors advisor, for helping me to complete my degree requirements and to begin my thesis.

I thank my friends for their dauntless determination and my family for their endless encouragement.

Elizabeth Kowalski
University Park, PA
April 2, 2008

This research was supported by the National Science Foundation under grants ATM-0652148 and ATM-0734083 to The Pennsylvania State University.

Dedication

to my father,

John Kowalski,

“Next year will be easier.”

Chapter 1

Introduction

1.1 Importance of Corona

When Benjamin Franklin invented lightning rods, he believed that the sharp tips on his metal rods would prevent lightning discharge to the ground by discharging thunderclouds. However, he discovered that his sharp-tipped lightning rods had the opposite effect. Instead of eliminating lightning from the sky, his rods attracted lightning. Inspired by this discovery, lightning rods were used to direct lightning safely to the ground and away from tall structures. Since its invention, the design of the lightning rod has changed little [*Uman*, 2001, pp. 5–8 and references cited therein].

Since Benjamin Franklin's time, scientists have developed a better understanding of the lightning process. The charge that accumulates in a thundercloud causes an increase in the ambient electric field at the ground. This field can be greatly increased (typically by about 1–2 kV/cm [*Moore et al.*, 2003]) at the top of tall, grounded, objects, e.g., the tip of a lightning rod, the roof of a building, or the top of a tree, due to the sharp change in voltage between the object and the

surrounding atmosphere. If cloud-to-ground lightning descends from the thundercloud, the electric field will increase even more. The large electric field causes a current to flow through these objects, accumulating charge that forms a so-called corona around the top. From the corona, upward, needle-like ionizations channels, first as non-thermal "streamers" and, subsequently, as thermalized "leaders", can develop. This process will be described in further detail below. Eventually, a downward leader from cloud-to-ground lightning will meet an upward leader from the ground, connecting the cloud-to-ground lightning to the ground [e.g. *Bazelyan*, 2007; *Aleksandrov et al.*, 2005b; *Bazelyan and Raizer*, 2000, pp. 1–10].

In the specific case of a lightning rod, a corona forms during a slow rise of voltage on the rod. The rise in voltage can be due to charge build up in the thundercloud, previous lightning in the surrounding area, or a downward leader descending from the thundercloud. When the electric field near the tip of the rod reaches the critical electric field for ionization ($\approx$ 43 kV/cm at ground pressure), corona is initiated. At this critical electric field, an ionization layer forms at the edge of the rod-tip, which injects a current into the surrounding air. The charge density of the developing corona around the tip of the lightning rod is typically on the order of 10^{15} m^{-3} [e.g., *Becerra et al.*, 2007; *Aleksandrov et al.*, 2005b; *Bazelyan and Raizer*, 1998, pp. 72–75, and discussion therein].

After a corona has formed around the tip of a lightning rod due to a slow voltage rise, a streamer can be initiated. A streamer is a string of progressively avalanching charge that appears and disperses quickly. Streamers are characterized as having a constant internal electric field of about 4.5 kV/cm. A streamer is initiated from the tip of a lightning rod when the electric field near the tip becomes strong enough to support ionization outside of the edge. The required electric field is defined by the combination of the Townsend criteria (for initiation) and the Meek criteria (for

development) [see *Meek and Craggs*, 1978, pp. 392–394; [*Raizer*, 1991, pp. 345–347; *Bazelyan and Raizer*, 2000, pp. 32–58; *Cooray*, 2003, pp. 70–79].

The streamer–leader transition occurs when the temperature increase produced by streamers becomes large enough to support thermal ionization. A leader is a plasma channel with a higher level ionization than streamers that forms along the length of an established streamer. It is characterized as conductive (with almost no voltage drop along its length), quick-forming (10^{-5}–10^{-6} s), and long-lasting [*Raizer*, 1991, pp. 363–367]. When streamers form, they typically stem off of the same point. As the voltage rises, the streamer corona and, subsequently, the concentration of streamers around an initiation point (the tip of a leader or a lightning rod) grows. Thermal ionization occurs when the concentration of streamers is strong enough to reach temperatures of ∼5000 K. At this point, the strongly ionized gas creates a thermal plasma channel that grows along the length of a streamer channel [*Raizer*, 1991, p. 365; *Bazelyan and Raizer*, 2000, pp. 59–61]. Another form of ionization occurs when the collective current of streamers is strong enough to produce a temperature of about 2000 K. At this temperature, electron detachment from O_2^- ions occurs in atmosphere. This detachment process forms a leader [*Raizer*, 1991, pp. 363–367; *Cooray*, 2003, pp. 82–84]. Experiments have shown that leader initiation occurs typically when streamers reach a length of about 1 m [e.g., *Raizer*, 1991, p. 366; *Becerra and Cooray*, 2006a]. This can also be characterized as a 400-kV voltage drop along the length of a 1-m long streamer [e.g., *Aleksandrov et al.*, 2002; *Aleksandrov et al.*, 2005b].

Paradoxically, the corona that develops around a lightning rod often serves to prevent the initiation of upward streamers and leaders. Studies have shown that, when a corona is present, a longer time is needed for streamer and leader initiation [*Becerra and Cooray*, 2006b; *Aleksandrov et al.*, 2005b; and Chapter 4

of this thesis]. This shielding effect is due to the charge of the corona preventing the electric field from growing to satisfy the Meek criterion for streamer initiation. Also, the corona charge limits the length of streamers formed, which delays the leader formation [*Becerra and Cooray*, 2006b]. For this reason, an appropriate understanding of the corona around lightning rod tips is necessary.

With an appropriate understanding of lightning and corona, it is possible to create a better lightning rod. It has been suggested that a blunt-tipped rod may attract lightning more than Franklin's sharp-tipped rod because of the different electric fields and coronas that the tips produce [*Moore et al.*, 2000b; *Becerra and Cooray*, 2006b, and references cited therein]. Electromagnetic modes exist [see Chapters 2 and 4] to quantify the electric field that surrounds a lightning rod, the corona that develops around a lightning rod in thunderstorm conditions, and the conditions of upward leader initiation from the tip of a lightning rod. By analyzing the model equations, the striking distance of different types of lightning rods can be determined. However, these equations are mostly empirical and practical applications involve complex time-dependent variables, such as charge density development and dynamic electric field, that are difficult or impossible to compute analytically.

The optimum lightning rod tip configuration has been explored by recent studies involving the analysis of time-dependent electric fields and the development of complex and time consuming numerical models (to be discussed in the following section). Typical rod tip configurations in these studies involve sharp or blunt tips with various radii, typically 1–125 mm. A debate has risen about how much more protection an optimum lighting rod tip will offer. An optimum rod tip radius could lead to better protection of structures from lighting. As it is now, no model exists to adequately relate lightning rod tip-radii to strike-receptiveness.

1.2 The Effects of Lightning Rod Tip Radius on Strike-Receptiveness

1.2.1 Field Studies

Field studies about lightning rods are useful because they show practical results of different lighting rod tip configurations on strike-receptiveness. Though measurements from these studies are difficult to obtain, they show the most realistic values. Only one major field study has been performed because of the large amount of time needed to collect data.

For seven years, *Moore et al.* [2000a] studied the strike-receptiveness of sharp- and blunt-tipped rods placed on the summit of South Baldy Peak in New Mexico. In this competition between rods, *Moore et al.* [2000a] attempted to show the effectiveness of different rod types. Blunt-tipped rods were constructed with hemispherical tips ranging from 9.5 mm to 51 mm in diameter. On the summit, traditional sharp-tipped Franklin rods were mounted with blunt-tipped rods placed 6 m away from each Franklin rod.

In their study, *Moore et al.* [2000a] found that blunt-tipped rods were more likely to be struck by lightning. In seven years, they observed 12 lightning strikes to the rods. The 19-mm diameter lightning rods were struck the most often, while none of the sharp-tipped rods were ever struck. This data indicated a clear advantage of the blunt-tipped rods over the sharp-tipped rods used in this study.

In addition, current measurements were taken from both a sharp- and blunt-tipped rod for three specific nearby lightning strikes. The first and second lightning strikes occurred in the observed area and caused large currents of over 8 A in the blunt-tipped rod and relatively small currents (less than 2 A) in the sharp-tipped

rod. For the third strike, which occurred 10 meters closer to the sharp-tipped rod than the blunt-tipped rod, the sharp-tipped rod had the greater current of 3.7 A, while the blunt-tipped rod had a current of about 3 A.

Moore et al. [2000a] conducted the first long-term, accurately documented, field study about the strike-receptiveness of sharp- and blunt-tipped lightning rods. From this study, it could be conclusively said that, when placed in direct competition, *Moore et al.* [2000a]'s blunt-tipped rods were better than their sharp-tipped rods at attracting lightning. It remains to be explored, though, how these rods perform when in practical use rather than on a clear summit with few other ground obstructions [*Bazelyan*, private communication, 2007]. Also, the quantification of a rod's strike-receptiveness and the significance of differences between sharp- and blunt-tipped lightning rods remained to be explored. Though the electric field around rod tips was merely glanced over, it was clear from this study that calculations of electric field would prove useful in quantifying a rod's strike-receptiveness.

Recognizing the need to further explore the effect of ambient electric field on strike-receptiveness, *Moore et al.* [2000b] published a complementary article to the experiment described above. Using the same competition between sharp- and blunt-tipped rods as *Moore et al.* [2000a] for data, *Moore et al.* [2000b] analytically calculated the electric field around similarly-shaped ellipsoids in order to further explain why only blunt rods were struck in the competition.

The calculations of electric field quantified *Moore et al.*'s [2000a; 2000b] results that their blunt-tipped rods were more strike-receptive than sharp-tipped rods. *Moore et al.* [2000b] found that the electric field around sharp-tipped rods was intensified by over twice as much at the surface of the tip. However, *Moore et al.* [2000b] also observed that the electric field surrounding blunt-tipped rods dropped less rapidly with distance than the electric field around sharp-tipped Franklin rods

[*Rison*, private communication, 2007]. For a rod with a 10-mm radius, the blunt-tipped electric field became greater at about 0.8 cm away from the tip. This observation meant that blunt-tipped rods had greater electric fields at distances more than a few centimeters away from the tip of the rod, which could make them more receptive to lightning.

Moore et al. [2000b] related electric field to strike-receptiveness in order to explain why only blunt-tipped rods were struck in their field study. An electric field above a certain threshold value (about 4.3 kV/cm) allowed upward streamer and leader initiation from the tip of the rod. Therefore, the blunt-tipped rod's larger electric field over a longer distance than the sharp-tipped rod allowed for longer upward leaders. Longer upward leaders led to an increase in the protection radius of the blunt-tipped rod.

In attempting to isolate the reason behind why no Franklin rods were struck in the field study, *Moore et al.* [2000a] and *Moore et al.* [2000b] showed that the electric field can be directly correlated to strike-receptiveness. However, using ellipsoids to represent rods, produced estimation errors. By using a numerical approach to solve for electric field, these errors can be reduced, as seen in Section 1.2.3.

1.2.2 Laboratory Experiments

Although field studies can provide the most accurate information on strike-receptiveness, laboratory studies provide a way to obtain useful data while operating in conditions close to those of practical interest. While field studies take years to observe natural lightning strikes, laboratory studies can simulate lightning on command. However, the laboratory environment does not always accurately reproduce

real situations and may lead to unreliable results.

Moore et al. [2003] built upon their previous results on competition between sharp- and blunt-tipped rods [*Moore et al.*, 2000a; *Moore et al.*, 2000b] to analyze strike-receptiveness. They explored the electric field surrounding lightning rods in order to provide an explanation for the differences observed between strike-receptiveness.

In the experiment, *Moore et al.* [2003] electrically simulated thunderstorm conditions for a sharp- and a blunt-tipped lightning rod. They placed the lightning rods in a strong electric field of about 100 kV/m. In the electric field, a sharp-tipped rod produced a blue glow that extended from the tip to 5–7 mm away. Meanwhile, a blunt-tipped rod (19-mm diameter) produced a more erratic glow up to 70 mm away with streamers that extended to the generator electrode, located 40 cm away.

Moore et al. [2003] explained these glows as corona and developed a reason for strike-receptiveness. The glow observed around the lightning rod was due to avalanching electrons created by the enhanced electric fields at the tip of the rod. Since the blunt-tipped rods had a larger electric field over a longer distance, the glow for those rods extended over 60 mm farther than the glow for sharp-tipped rod. This longer distance was enough for the blunt-tipped rods to create streamers that extend past the corona to the generator electrode. However, the sharp-tipped rod did not create a large enough corona to create streamers. Therefore, *Moore et al.* [2003] concluded that blunt-tipped rods were better strike receptors than sharp-tipped rods because a blunt-tipped rod allowed for the initiation of streamers at lower ambient electric fields. However, the exact values of electric field were not given. By investigating various rod tip radii, *Moore et al.* [2003] concluded that the optimum diameter for a blunt-tipped rod was between 12.7 mm and 19 mm.

This study provided an important link between electric field and strike-receptiveness. *Moore et al.* [2003] demonstrated that the development of streamers is due to the observed corona that, in turn, is due to the enhancement of the electric field at the tip of a rod [*Raizer*, 1991, pp. 345–347]. In providing this link, the protection of a lightning rod in an undisturbed electric field can be quantified by how much a lightning rod enhances the electric field in the area near its tip. The optimum diameter found with this approach was within the range of rods struck by lightning in *Moore et al.* [2000a], indicating the validity of this approach.

Citing a lack of data in *Moore et al.* [2000a], *D'Alessandro et al.* [2003b] performed a large-scale laboratory experiment to test the difference in strike-receptiveness between sharp- and blunt-tipped rods. Using a laboratory set-up to imitate *Moore et al.*'s [2000a] field study, they hoped to provide large amounts of data on strike-receptiveness. They hoped that the quantity of data provided in the laboratory experiment would allow statistically significant conclusions to be drawn.

D'Alessandro et al. [2003b] used two different laboratory settings to put sharp- and blunt-tipped rods in competition. First, they placed a sharp-tipped rod (radius 0.2 mm) and a blunt-tipped rod (radius 12.5 mm) 3 m apart with a plane generator electrode 5 m overhead. Electric pulses were sent through the plane electrode and the number of strikes to each rod was recorded. Next, this experiment was repeated with a rod electrode placed 3 m overhead.

The results for this study were inconclusive in indicating strike-receptiveness. For the first experiment, the sharp-tipped rod was slightly more receptive to strikes than the blunt-tipped rod, receiving 45 and 39 hits of 60 pulses tested for two different rod heights. However, when the distance between rods was increased to 6 m for the same experiment, the sharp-tipped rod received only 21 hits of 40 pulses.

Also, for the second experiment, the rods performed equivalently. Out of 200 pulses, the sharp- and blunt-tipped rod received 69 and 63 hits, respectively. The difference in hits to sharp- and blunt-tipped rods were so small that no conclusions could be drawn.

Although *Moore et al.* [2000a; 2000b; 2003] showed that blunt-tipped rods had an advantage over sharp-tipped rods, the *D'Alessandro et al.* [2003b] study was important because it demonstrated that the advantage may not be as significant as *Moore et al.* had indicated.

Ahmad and Ong [2005] performed a laboratory experiment to relate strike-receptiveness and the ionization breakdown parameters of various lightning rods. They measured the breakdown voltage and breakdown time (the time until ionization occurs when placed under a consistent voltage) of lightning rods with standard, sharp, blunt, flat, conical, and concave tips. Standard tips are defined in this article as a sharp tip with the point flattened. To test the relation between strike-receptiveness and the measured breakdown parameters, *Ahmad and Ong* [2005] placed standard-, blunt-, and sharp-tipped rods in competition with each other.

Ahmad and Ong [2005] believed that a rod with a low breakdown voltage and a long breakdown time would be the most strike-receptive. With that hypothesis, the breakdown parameters were measured for individual rods. The blunt-tipped rod had the lowest breakdown voltage of $\sim$1450 kV. The breakdown voltages for the standard- and sharp- tipped rods were only $\sim$20 kV higher. All other rods had significantly higher breakdown voltages. The blunt-tipped rod also had the longest breakdown time of $\sim$12 μs. However, all other rods had breakdown times within 3 μs.

To test if having the lowest breakdown voltage and the longest breakdown time would give the blunt-tipped rod an advantage, *Ahmad and Ong* [2005] tested this

rod against the standard- and sharp-tipped rods. They placed two competing rods (either blunt- and sharp-tipped or blunt- and standard-tipped) 2 m apart, and a generator electrode 2 m overhead of the midway-point between the rods. The generator electrode was charged repeatedly, and the number of electric strikes to each rod was recorded. When placed in competition with the sharp-tipped rod, the blunt-tipped rod received 70% of the strikes; when placed in competition with the standard-tipped rod, the blunt-tipped rod received 60% of the strikes. These results further develop the debate between sharp- and blunt-tipped rods.

1.2.3 Computer Models

With computer simulations of strikes to lightning rods, it is possible to analyze strike-receptiveness with a large amount of data in a controlled environment. Computer simulations use established equations in their approaches, though large errors can still occur due to approximations and idealizations. Because they are restricted to known equations, simulations may be over-simplified to accurately represent reality. However, simulations are often used with laboratory parameters or settings. We note that in the model studies reported in this thesis, a sphere with radius of 1 mm is used to represent a sharp-tipped rod.

In an effort to quantify strike-receptiveness, *D'Alessandro* [2003a] developed a computer simulation to calculate the striking distance of lightning rods with varying input parameters. In his numerical approach, *D'Alessandro* [2003a] placed a blunt-tipped rod of specified height and radius on a rectangular or cylindrical structure or on a flat surface. He introduced a downward leader into the simulation and calculated the upward leader development from the lightning rod as function of time. Using the time of upward leader initiation, striking distance was found as

a function of the input parameters.

D'Alessandro [2003a] found that both rod tip radius and rod height affected striking distance of a lightning rod. For rods less than 2 m high placed on a flat surface, the rod tip radius caused little effect on striking distance. However, as rod height increased to 8 m and above, the rod tip radius had an increasing non-linear effect on striking distance. Similar measurements were taken for rods placed on rectangular and cylindrical structures. From all simulations, the largest striking distances occur for tip radii between 0.01 m and 0.1 m.

Improving on *D'Alessandro* [2003a], *D'Alessandro* [2007] calculated the optimum lightning rod tip radius. Solving for ambient electric field, he calculated the optimum rod radius using two criteria: the point of corona inception and the strength of electric field above the ionization region. However, *D'Alessandro* [2007] did not discuss how these values were used to determine the optimum radius.

The results from *D'Alessandro* [2007] corresponded to the experimental setting of *Moore et al.* [2000a] and illustrated the dependency of a lightning rods strike-receptiveness on its surroundings. When *D'Alessandro* [2007] simulated parameters similar to *Moore et al.*'s experimental set-up, the optimum radius was 8–10 mm. In *Moore et al.*'s study, lightning most often struck 19-mm-diameter (9.5-mm radius) rods. *D'Alessandro* [2007] also showed that the optimum rod radius could be proportionally dependent on the height of the rod. Other input parameters, such as the structure on which the rod was placed and the placement of the rod on that structure showed no definite effects on rod radius. Overall, the optimum rod tip radius rarely exceeded 30 mm.

D'Alessandro's [2007] studies are incomplete because the optimum rod tip radius was calculated with no indication of how much the rod tip radius affected a lightning rod's performance. Though the optimum rod radius would clearly have

the largest protection radius, how much larger this protection radius is than that of other rod radii remains unanswered. However, the validation of *Moore et al.*'s [2000a] field study indicated that the effects of a blunt-tipped rod's radius on strike-receptiveness should not be completely ignored.

Adopting a simpler simulation domain, *Aleksandrov et al.* [2005a] simulated a 1–D spherical approximation of a lightning rod in thunderstorm conditions in order to quantify a rod's performance. This model was developed from previous work on corona discharges [*Aleksandrov et al.*, 2002]. The 1–D estimation of a lightning rod as a sphere was justified by a less than 20% error and yielded a simple model. *Aleksandrov et al.* [2005a] numerically calculated the dynamic corona due to the enhancement of electric field.

The dynamic corona calculations revealed little dependence of a lightning rod's protection distance on tip radius. From the dynamic corona, *Aleksandrov et al.* [2005a] determined the height of a descending downward leader that would initiate upward streamers and form leaders from the tip of a lightning rod. They observed that, though the initiation of streamers depends slightly on rod radius, the height of initiation of a connecting leader has negligible dependence. For a rod tip radius less than 1 cm, the upward leader was initiated around 460 m. For all simulated rod tip radii, the upward leader was initiated between 300–475 m. A range of 175 m was small compared to the size of thunderstorms (on the magnitude of kilometers). From these results, *Aleksandrov et al.* [2005a] concluded that rod tip radius had little effect on striking distance. In addition, *Aleksandrov et al.* [2005b] and *Aleksandrov et al.* [2006] used the same simulation to explore how corona affected the strike-receptiveness of a lightning rod, concluding that the discharge process was "almost independent of the hemisphere radius."

Bazelyan et al. [2008] reviews the work of *Aleksandrov et al.* [2002], *Aleksan-*

drov et al. [2005b], and *Aleksandrov et al.* [2006] on non-stationary corona models. *Bazelyan et al.* [2008] discusses a 1–D non-stationary corona and upward leader formation model. In the model, simplifications render the calculations nearly independent of radius. The effect of radius on leader formation is not considered pertinent because leader formation is approximated to be independent of radius.

1.3 Problem Statement

This thesis investigates the corona development between spherical electrodes to draw conclusions about the most effective lightning rod tip radius. By simulating streamer and leader initiation from non-stationary corona, the relationship between inner electrode radius and leader initiation is established. This model is used to discuss the strike-receptiveness of sharp and blunt-tipped lightning rods.

The one-dimensional spherical simulation that was developed by *Aleksandrov et al.* [2005a] and further used and explained by *Aleksandrov et al.* [2005b], *Aleksandrov et al.* [2006], and *Bazelyan et al.* [2008] is inaccurate. Although the simulation that they present is correct in its derivation, it is missing several key points that should be addressed. The simulation must be taken one step further and include the development of streamer corona and the leader initiation in order to adequately assess the strike-receptiveness of lightning rod tips.

The model in this thesis uses a one-dimmensional spherical geometry to represent a lightning rod, similar to that discussed by *Bazelyan et al.* [2008]. To explain the physical development of this spherical approach, a simple diagram of a lightning rod is shown in Figure 1.1(a). Here, the lightning rod is in a uniform electric field. The voltage difference between the tip of the grounded rod and the surrounding air is indicated as $\Delta U = E_0 h$. This abrupt change in voltage is due

to the fact that the voltage on the grounded rod is 0 V, and the voltage of the atmosphere is defined through the uniform ambient electric field as $U(z) = -E_0 z$ (where z indicates height). Another diagram, Figure 1.1(b), models this same rod as a sphere with a voltage of $U = E_0 h$. The ground plane can be eliminated with minimal error when one is considering only the space above the lightning rod [cf. *Aleksandrov et al.*, 2005a], leaving a sphere in free space (as shown in Figure 1.1(c)).

Finally, an outer spherical electrode must be added in order to limit the scope of the simulation domain. Figure 1.1(d) shows the physical diagram of the simulation domain. The rod radius (as defined by the inner electrode radius, R_1) is variable, while the outer electrode radius, R_2, is meant to be kept consistently far away (unless otherwise specified). In the limit as R_2 approaches infinity, the model becomes a sphere in free space (Figure 1.1(c)). The voltage on the rod is the same as the applied voltage between the inner and outer electrodes, U. The applied voltage will be defined separately for each simulation. The spherical symmetry of this one-dimentional (1–D) model allows it to be dependent only on spherical radius, r. As specified on Figure 1.1(d), Δr represents the distance between grid points in r, which are introduced for a numerical solution of the problem.

The model simulates the development of corona around the inner radius. Corona develops around a conductor when the electric field near the surface of the conductor becomes greater than the critical electric field for corona initiation. According to *Bazelyan et al.* [2007] and *Bazelyan et al.* [2008] this can be estimated empirically as

$$E_c = 27.8 \left(1 + \frac{0.54}{\sqrt{100 R_1}}\right), \tag{1.1}$$

where E_c and R_1 are in units of V/m and m, respectively. This corona develops

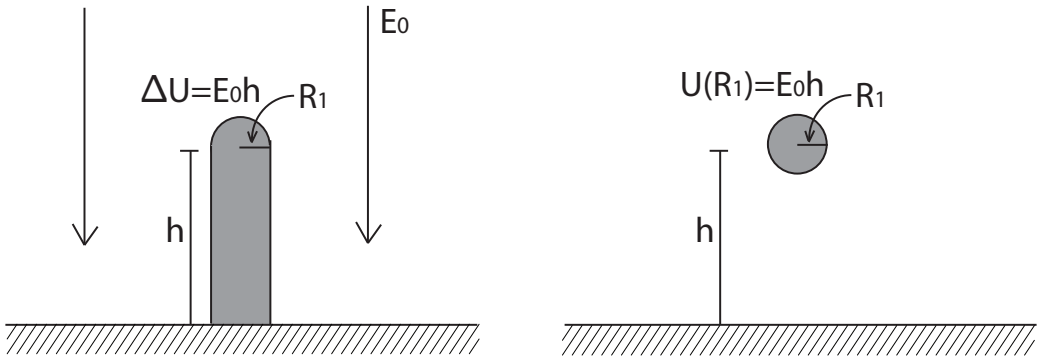

(a) Axisymmetric lightning rod.

(b) Effective representation of lightning rod with a sphere.

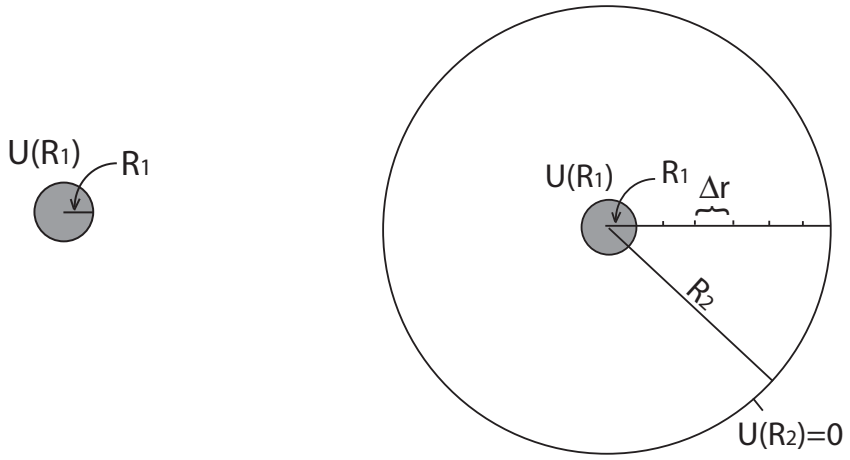

(c) Removal of the ground plane.

(d) One-dimmensional model.

Figure 1.1. Progression of the physical model from an axisymmetric lightning rod to one-dimensional spherical electrodes. See text for details.

because the electric field in the ionization region cannot exceed the critical value, E_c, but the applied voltage must be compensated. The ionization region is viewed as a narrow region on the surface of the conductor with the ability to feed a current of positive ions into the system [*Aleksandrov et al.*, 2002]. In the physical

model dipicted by Figure 1.1(d), the electric field reaches this critical value, E_c, when the applied voltage between the electrodes exceeds U_c (such that $E(R_1) = E_c$ without corona considered). In the given situation, the inner electrode acts as a grounded conductor because it represents a grounded lightning rod. A time-dependent corona will develop around the inner electrode, eventually expanding to fill the entire simulation domain [e.g., *Roth*, 1995, pp. 251–256].

The stationary (or steady-state) and non-stationary (or time-dependent) corona development between the spherical electrodes is simulated in this thesis. In the stationary case, well-established electromagnetic equations are employed and a numerical solution is obtained and validated. The stationary case is used as a basis for the development of non-stationary corona model and as a means of validation of this model.

The non-stationary corona model can be used to track the streamer and leader development from the inner electrode. Using established initiation criteria for streamers and leaders, the time and length of streamer corona and the moment of time of leader initiation can be found through the model. These results can be related to the radius of the inner electrode and used to draw conclusions regarding optimum lightning rod tip radius.

1.4 Organization of this Thesis

Chapter 1 provides an introduction to lightning and corona effects as well as a review of the literature on studies that have been done to investigate the effect of lightning rod tips on strike-receptiveness. Section 1.3 provides a basis for the one-dimentional spherical model of corona. Chapter 2 introduces stationary corona, develops a related simulation model, and validates the approach. In Chapter 3,

non-stationary corona are introduced and a related simulation model is developed. Streamer and leader initiation criteria are added and a relationship is established between the time of leader initiation and the inner electrode radius. Chaper 4 discusses the results of the non-stationary simulations. The non-stationary corona and lightning model are validated and discussed. Finally, Chapter 5 drawa conclusions from both stationary and non-stationary models and suggest future research.

Chapter 2

One-Dimmensional Spherical Models of Stationary Corona

In order to develop a time-dependent simulation, the stationary approach must first be considered. In this approach, Figure 1.1(d) was used as the physical basis. In this Chapter, $U(t) = U_0$, a constant value with respect to time.

2.1 Development of the Models

The stationary solution was found for two different approximations. First, the ion density (or corona), n, between the spheres was taken to be a constant value with respect to r, (i.e., $n = \text{const}$). Then, the solution was improved for an ion density dependent on r (i.e., $n = n(r)$). The adapted method of corona analysis was based on the approaches by *Roth* [1995, pp. 256–260] and *Aleksandrov et al.* [2002]. Similar stationary corona analysis was also discussed in, e.g., *Bazelyan et al.* [2007] and *Becerra et al.* [2007]. The analysis from *Roth* [1995, pp. 256–260] has been adapted to spherical coordinates and expanded to involve a numerical

solution for the variable ion density approach.

2.1.1 Model Using a Constant Ion Density

In this first approach, the ion density is kept independent of radius as well as time, $n = \text{const}$. In other words, between the electrodes: $dn/dt = 0$ and $dn/dr = 0$.

When there is no corona ($n = 0$), the electric field and voltage equations for all space can be found easily. This solution corresponds to a situation when the voltage applied to the spheres is below the critical voltage required for corona initiation, U_c. In this case,

$$E(R_1) < E_c \tag{2.1}$$

and

$$U_0 < U_c, \tag{2.2}$$

where E_c is defined in Equation (1.1).

Solutions for the voltage and electric field with respect to distance, r, can be found using Poisson's equation, $\nabla^2 U = 0$. Boundary conditions were taken such that $U(R_1) = U_0$ and $U(R_2) = 0$, so that

$$U(r) = \frac{U_0 R_1 R_2}{(R_2 - R_1)} \frac{1}{r} - \frac{U_0 R_1}{(R_2 - R_1)}. \tag{2.3}$$

From here, electric field can be found as

$$E(r) = -\frac{dU}{dr} = \frac{U_0 R_1 R_2}{R_2 - R_1} \frac{1}{r^2}. \tag{2.4}$$

The critical voltage, U_c will be defined at the point where $E(R_1) = E_c$. With

electric field and voltage defined, U_c is determined as

$$U_c = \frac{R_1}{R_2} E_c (R_2 - R_1). \tag{2.5}$$

This value can be used to determine what voltage must be applied to the electrodes in order to initiate corona into the system. We note that it is independent of ion density assumptions. We note also that, in a limiting case where $R_2 >> R_1$, $U_c = R_1 E_c$.

Once the voltage on the sphere is increased beyond the critical voltage for corona initiation, i.e., $U_0 > U_c$, the problem changes as a corona develops and $n \neq 0$. Therefore, n must be taken into account when calculating $U(r)$ and $E(r)$. In this case, the analysis will be determined by ion density assumptions. Due to breakdown considerations, the electric field at the surface of the inner sphere remains at a constant value, E_c, despite any further increase in potential [*Aleksandrov et al.*, 2002]. The iteration procedure, explained below, to obtain a solution under the constant ion density assumption closely follows steps explained in *Raizer* [1991, pp. 345–352]].

To begin, the current is defined using current density,

$$\vec{J} = \rho \vec{v}, \tag{2.6}$$

the velocity of ions,

$$\vec{v} = \mu_i E, \tag{2.7}$$

and the definition of current,

$$I = \iint \vec{J} \cdot \, d\vec{S} = 4\pi r^2 J. \tag{2.8}$$

By combining the these equations, the current is defined for the spherical domain as

$$I(r) = 4\pi r^2 q_e n \mu_i E. \tag{2.9}$$

Using Equation (2.4)—keeping in mind that this electric field definition applies to a situation with no corona—and Equation (2.9), the density (as a constant value, independent of r) can be defined as

$$n = \frac{I(R_2 - R_1)}{4\pi q_e \mu_i R_1 R_2 U_0}. \tag{2.10}$$

The solution (2.4) for electric field remains approximately valid if the ion density is negligibly small. In order to find a more accurate solution for the electric field (i.e., to find the next iteration), Gauss's Law is written as

$$\vec{\nabla} \cdot \vec{E} = \frac{\rho}{\varepsilon_0} \tag{2.11}$$

can be applied for spherical coordinates, such that

$$\frac{1}{r^2}\frac{\partial}{\partial r} r^2 E(r) = \frac{\rho}{\varepsilon_0} = \frac{q_e n}{\varepsilon_0}. \tag{2.12}$$

From Equation (2.12), both sides can be multiplied by r^2 and integrated so that

$$r^2 E(r) = \int r^2 \, \frac{q_e n}{\varepsilon_0} \, dr. \tag{2.13}$$

Integration results in

$$r^2 E(r) = \frac{q_e n}{\varepsilon_0} \, \frac{r^3}{3} + C. \tag{2.14}$$

The integration constant, C, in Equation (2.14) is defined such that Equation (2.4)

is consistent at R_1 when $U(R_1) = U_0 = U_c$. (This definition is because electric field is always equal to E_c as defined by Equation (1.1) on the inner electrode's surface, $E(R_1) = E_c$.) That is, at the point of corona inception, the electric field defined by Equations (2.4) and (2.14) will be equivalent. Therefore, C is defined such that

$$E(r) = \frac{q_e n}{3\varepsilon_0} \frac{r^3 - R_1^3}{r^2} + \frac{R_1 R_2 U_c}{r^2(R_2 - R_1)}. \tag{2.15}$$

From Equation (2.15), Poisson's Equation can be used to find voltage on the inner electrode from the electric field as

$$U = \int_{R_1}^{R_2} E(r)\, dr, \tag{2.16}$$

$$U = \int_{R_1}^{R_2} \frac{q_e n}{3\varepsilon_0} \frac{r^3 - R_1^3}{r^2} + \frac{R_1 R_2 U_c}{r^2(R_2 - R_1)}\, dr. \tag{2.17}$$

Solving Equation (2.17), yeilds

$$U = \frac{q_e n}{3\varepsilon_0} \left(\frac{R_2^2 - R_1^2}{2} \right) - \frac{q_e n}{3\varepsilon_0} R_1^3 \left(\frac{R_2 - R_1}{R_1 R_2} \right) + U_c. \tag{2.18}$$

Using Equation (2.10) to substitute for n in terms of current, the potential can be found as a function of current. Solving for current as a function of potential, the current–voltage characteristic of the system can be defined as

$$I = \frac{24\pi\varepsilon_0 \mu_i R_1 R_2^2}{(R_1 - R_2)^2 \left(R_2^2 + R_1 R_2 - 2R_1^2\right)} U(U - U_c). \tag{2.19}$$

In the limit as R_2 approaches infinity, meaning that the inner electrode exists

in free space (see Figure 1.1(c)), this solution approches

$$I = 24\pi\varepsilon_0\mu_i\frac{R_1}{R_2^2}U(U - U_c). \tag{2.20}$$

Equivalently, *Aleksandrov et al.* [2002] states Equation (2.19) as:

$$I = B\,U(U - U_c), \tag{2.21}$$

where B is stated only as a proportionality constant. With the above derivation, $B = 24\pi\varepsilon_0\mu_i\frac{R_1}{R_2^2}$ for the geometry being considered. *Moore et al.* [2000a, and references therein] state a mathematically equivalent current–voltage formula determined through experimental observations, also with undefined constants for B and U_c. Alternatively, Equation (2.19) clearly shows the dependence of this current–voltage relationship on the geometry of the system and ion mobility.

The analytical solution given by Equations (2.10) and (2.19) for a constant density, stationary corona between two spherical electrodes provides the ion density and current–voltage characteristics of the system.

2.1.2 Model Using a Variable Charge Density

Modifying the problem of the previous section, it is possible to find a more accurate solution for the stationary corona when the ion density is a function of radius, $n = n(r)$. In other words, we now consider the case when $dn/dt = 0$ and $dn/dr \neq 0$. Again, Figure 1.1(d) is used for these conditions. In this way, the electric field and voltage before corona initiation are defined by Equations (2.3) and (2.4), respectively. Likewise, E_c and U_c remain the same and are related by Equation2.5. Also, the definition of current is given by Equation (2.9).

Corona is initiated when $E > E_c$. To consider a variable ion density, the continuity equation can be considered. In this problem the continuity equation is simple due to the stationary, or steady-state condition

$$\frac{\partial \rho}{\partial t} + \vec{\nabla} \cdot \vec{J} = \vec{\nabla} \cdot \vec{J} = 0. \tag{2.22}$$

The current density for this problem can be defined as a function of electric field,

$$\vec{J} = \rho \vec{v} = n q_e \mu_i E. \tag{2.23}$$

Having combined Equations (2.22) and (2.23), a relation for $n(r)$ can be found

$$\frac{1}{r^2} \frac{\partial}{\partial r} \left[r^2 n q_e \mu_i E(r) \right] = 0. \tag{2.24}$$

Since the derivative must evaluate to 0, it is clear that a constant can be defined as

$$C = r^2 \underbrace{n q_e \mu_i E(r)}_{J}. \tag{2.25}$$

The integration constant, C, can be further defined through the definition of current density

$$C = r^2 J = r^2 \left(\frac{I}{4\pi r^2} \right) = \frac{I}{4\pi}. \tag{2.26}$$

Finally, the ion density can be solved as a function of r from Equation (2.25)

$$n(r) = \frac{I}{4\pi q_e \mu_i E(r) r^2}. \tag{2.27}$$

Using the established relations, the electric field can be derived as a function of I and r. Beginning with Gauss's Law for one-dimentional spherical coordinates,

and substituting Equation (2.27),

$$\frac{1}{r^2}\frac{\partial}{\partial r}r^2E(r) = \frac{nq_e}{\varepsilon_0} = \frac{I}{4\pi\varepsilon_0\mu_i E(r)r^2}. \tag{2.28}$$

Integrating both sides gives

$$\int r^2E(r)\,d(r^2E(r)) = \int \frac{I}{4\pi\varepsilon_0\mu_i}r^2\,dr, \tag{2.29}$$

which can be simplified to

$$\frac{(r^2E(r))^2}{2} = \frac{I}{4\pi\varepsilon_0\mu_i}\frac{r^3}{3} + C, \tag{2.30}$$

and solved for $E(r)^2$, such that

$$E(r)^2 = \frac{I}{6\pi\varepsilon_0\mu_i}\frac{1}{r} + \frac{2C}{r^4}. \tag{2.31}$$

The constant, C, in Equation (2.31) can be found by considering that electric field at R_1 is defined to be equivalent to the critical electric field, E_c,

$$E(R_1) = E_c = \frac{U_cR_2}{R_1(R_2 - R_1)}. \tag{2.32}$$

Combining Equations (2.32) and (2.31) and solving for C yeilds

$$C = \frac{1}{2}E_c^2\,R_1^4 - \frac{R_1^3\,I}{12\pi\varepsilon_0\mu_i}. \tag{2.33}$$

Finally, by substituting Equation (2.33) into Equation (2.31), a solution for $E(r)$

can be found,

$$E(r) = \frac{1}{r^2}\sqrt{E_c^2\, R_1^4 + \frac{(r^3 - R_1^3)\, I}{6\pi\varepsilon_0\mu_i}}. \tag{2.34}$$

Though a voltage–current characteristic cannot be found analytically, the voltage is still defined as the integral of electric field,

$$U(r) = \int_r^{R_2} E(r)\, dr, \tag{2.35}$$

where $U(R_2) = 0$. Specifically, the voltage on the inner electrode can be defined as

$$U(R_1) = U_0 = \int_{R_1}^{R_2} E(r)\, dr. \tag{2.36}$$

Using Equations (2.34) and (2.36), an analytical, closed form solution cannot be found. For this reason, the related solutions are not provided in the existing literature [e.g., *Roth*, 1995, p. 260; *Aleksandrov et al.*, 2002]. However, it is possible to find the current–voltage characteristics of this system numerically. Keeping in mind that the electric field is dependent on position, r, and current, the electric field and potential can be solved for a set of specific currents injected into the system. The related solution represents one of the original contributions of this thesis.

2.2 Results

Using the stationary corona equations from the previous section, an analytical solution for $n = const$ and a numerical solution for $n = n(r)$ were found. In order to obtain a numerical solution for stationary corona for the case when $n = n(r)$, a range of currents must be specified. The electric field, potential, and ion density

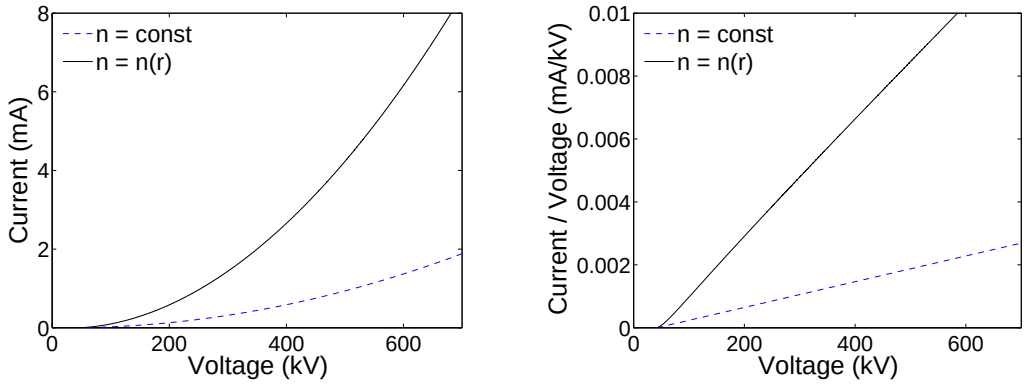

(a) (b)

Figure 2.1. Current–voltage characteristics of stationary corona for $R_1 = 0.01$ m and $R_2 = 0.5$ m. A linear relationship between I/V and V is obtained, as expected [*Raizer*, 1991, pp. 348–349].

must be calculated for each individual current. In order to numerically solve for potential via Equation (2.36), the dimension of the simulation domain must be discretized into a series of points that are Δr apart. The value of Δr is important for the integration of the electric field to find potential—a smaller Δr provides a more accurate solution.

For Figures 2.1–2.4, the parameters of the physical model (Figure 1.1(d)) were set as: $R_1 = 0.01$ m, $R_2 = 0.5$ m, and $\Delta r = 0.001$ m. With these parameters, $E_c = 43$ kV/cm and $U_c = 42.14$ kV ≈ 42 kV.

The current–voltage characteristics for both constant and variable ion density solutions are shown in Figure 2.1. The approaches are convergent around smaller voltages. The point where $I = 0$ A occurs when $U = U_c$, the limit of corona initiation. For any voltages lower than U_c, the electric field at R_1 is less than E_c. In these instances, there will be no initiated corona and, therefore, no current. That is: $I = 0$ A, for $U < U_c$. From the current/voltage vs. voltage plot, it appears that $I/V \propto V$ for both solutions.

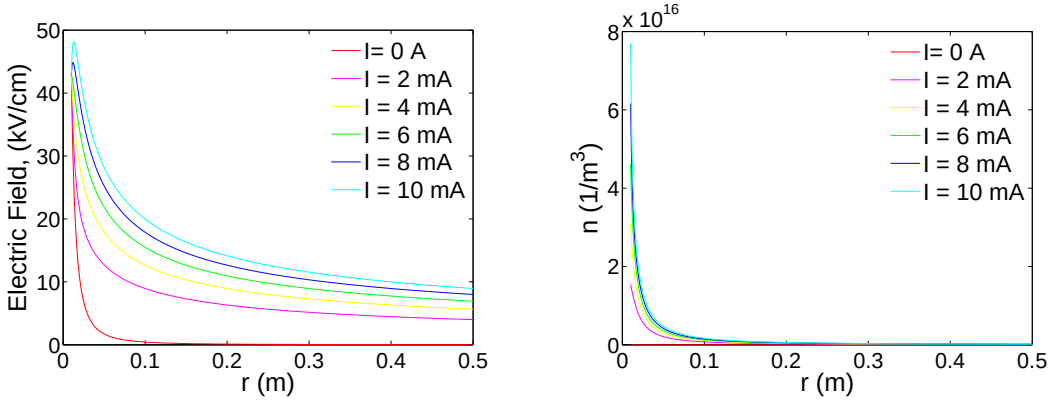

(a) (b)

Figure 2.2. (a) Electric field vs. position for various current values. $E(R_1) = E_c =$ 43 kV/cm for all displayed curves. (b) Ion density vs. position for various current values. $R_1 = 0.01$ m and $R_2 = 5$ m.

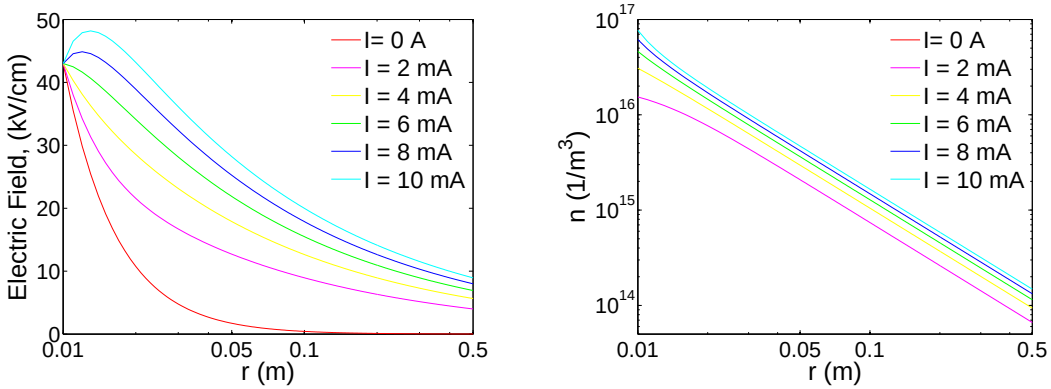

(a) (b)

Figure 2.3. (a) Electric field vs. position for various current values. $E(R_1) = E_c =$ 43 kV/cm for all displayed curves. (b) Ion density vs. position for various current values. Note that $r(m)$ and n are on a log scale to emphasize magnitudes of the values. $R_1 = 0.01$ m and $R_2 = 0.5$ m.

For the variable density model, the electric field and ion density as a function of radius were plotted for various currents in Figure 2.2. The electric field and ion density near the inner electrode are largely dependent on current. This dependence rapidly decreases with increasing distance away from the inner electrode.

Figure 2.3 shows the same data with radius on a logarithmic scale to emphasize the area close to the inner electrode. With ion density also plotted logarithmically, it is clear that ion density has a near-exponential dependence on radius. The logarithmic scale also makes observations about electric field possible near the inner electrode. For all currents, the electric field is kept at constant at R_1, following the boundary condition that $E(R_1) = E_c$. The electric field then decays rapidly from this point for low currents. However, for relatively high currents, the electric field increases before its decay. In Section 3.2, this observation about electric field will become an important point in non-stationary corona when discussing streamer initiation.

Figure 2.4 shows yet another way to look at electric field and ion density. These color scale images of one-dimensional data emphasize the concentration of electric field and ion density around the inner radius for one particular current, $I = 10$ mA. They reflect the explanation of corona by *Roth* [1995, pp. 253–255], and are characteristic of typical corona explanations. The ion density, particularly, is concentrated around the inner electrode and decays to relatively low density at the outer electrode. This is characteristic of a corona being concentrated around the sharp point in the system. Though it appears as if the ion density decays to zero at the outer radius, in actuality $n(R_2) \approx 10^{14}$ m^{-3}, as seen in Figure 2.3(b). In the stationary, steady-state, condition presented in Figure 2.3(b), the corona has pervaded the entire simulation domain. When considering non-stationary corona, an ion front will be visible before the solution settles. In this case, the ion density will be zero when downstream of the front of the corona. The corona front will advance due to the advancement of ions in the electric field, and will eventually reach the outer electrode. At this point, a steady-state solution will be established is illustrated in Figure 2.3(b).

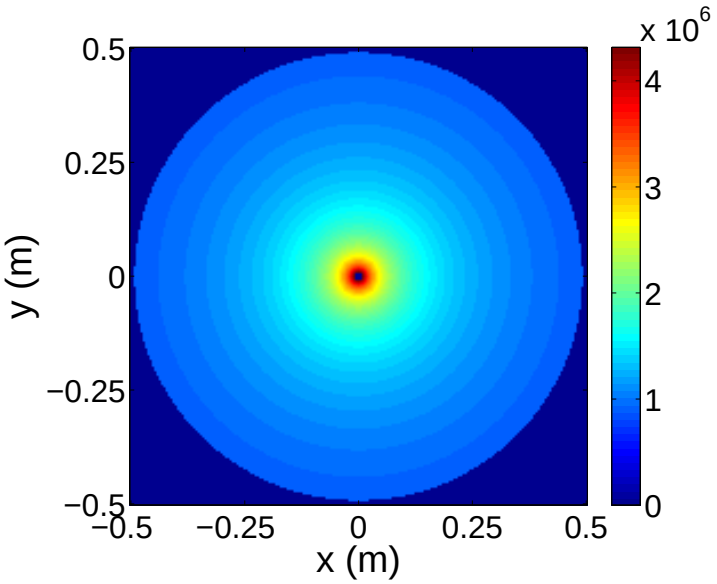

(a) Electric field (V/m)

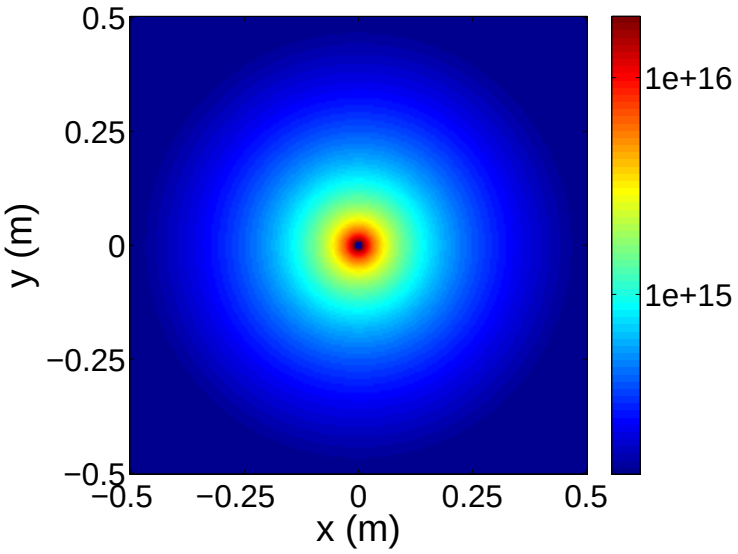

(b) Ion density $(1/m^3)$

Figure 2.4. Color scale images of the unidimensional non-stationary corona electric field and ion density at $I = 10$ mA for $R_1 = 0.01$ m and $R_2 = 0.5$ m. All points graphed which lie beyond $R_2 = 0.5$ m are taken as having a value of 0.

We note that solutions for constant and variable ion density shown in Figure 2.1 are in significant disagreement due to the obvious limitations of a constant

density assumption in a large gap. Intuitively, it could have been expected that the solutions for constant and variable ion density, stationary corona would converge for small gap geometries when $R_2 \approx R_1$. However, actual solutions for the small gap geometry discussed in this section reveal that, in practically significant cases of not very close R_1 and R_2, agreement is only achieved for small values of current. A simple explanation for this observation is provided by the analysis of Equations (2.27) and (2.34) in the limiting case $R_2 \approx R_1$.

According to Equations (2.27) and (2.34), the condition of near-constant ion density occurs only with relatively low currents. As estimated from Equation (2.34), these currents must be $\lesssim$ 14 mA, for $R_1 = 1$ cm and $R_2 = 1.1$ cm). This value comes from the requirements that the first term under the square root in Equation (2.34) should dominate the second one, such that

$$E_c^2 R_1^4 > \frac{(R_2^3 - R_1^3)\, I}{6\pi\epsilon_0\mu_i}. \tag{2.37}$$

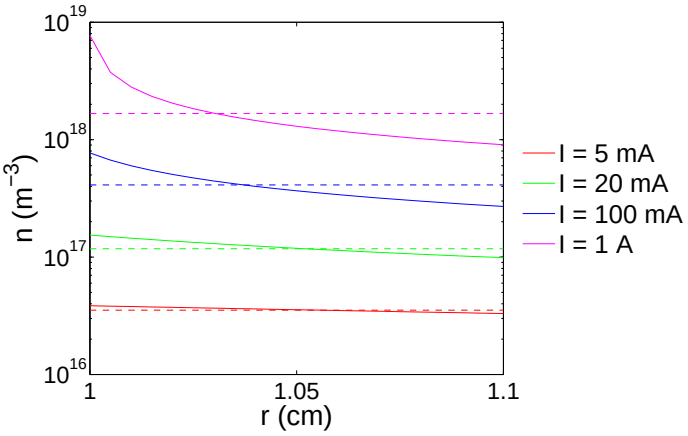

Figure 2.5. Ion density distributions for various currents. Comparable constant densities shown in dashed lines. Parameters of the model were $R_1 = 1$ cm and $R_2 = 1.1$ cm.

Under these conditions, Equation (2.34) can be simplified to

$$E(r) \approx \frac{E_c R_1^2}{r^2}. \tag{2.38}$$

Substituting Equation (2.38) into Equation (2.27) for variable ion density, the ion density can be simplified as

$$n(r) \approx \frac{I}{4\pi q_e \mu_i E_c R_1^2} \approx \text{const.} \tag{2.39}$$

At higher currents, the constant and variable ion density solutions will not converge. With the assumption of a large current, $E(r)$, as defined by Equation (2.34), can be approximated as

$$E(r) \approx \frac{1}{r^2}\sqrt{\frac{(r^3 - R_1^3)\, I}{6\pi\epsilon_0\mu_i}}. \tag{2.40}$$

This analysis yields an ion density from Equation (2.27) of

$$n(r) \approx \frac{I}{4\pi q_e \mu_i}\left(\frac{r^3 - R_1^3}{6\pi\epsilon_0\mu_i}\right)^{-1/2} \neq \text{const.} \tag{2.41}$$

In this case, ion density remains spatially dependent. Figure 2.5 illustrates that, in the spatially dependent ion density model, the ion density is nearly constant at low currents and significantly dependent on r at high currents.

The above analytical explanation is further supported by Figures 2.7 and 2.6, which illustrate the corresponding numerical solutions for a case when $R_2 \approx R_1$. We note that the solutions will not converge for large currents. This point is shown in Figure 2.7, where the constant and variable ion density solutions diverge for currents greater than $\sim$14 mA for the $R_2 - R_1 = 0.1$ cm gap considered. As also discussed above, the solutions will converge for small currents. Figure 2.6 illustrates

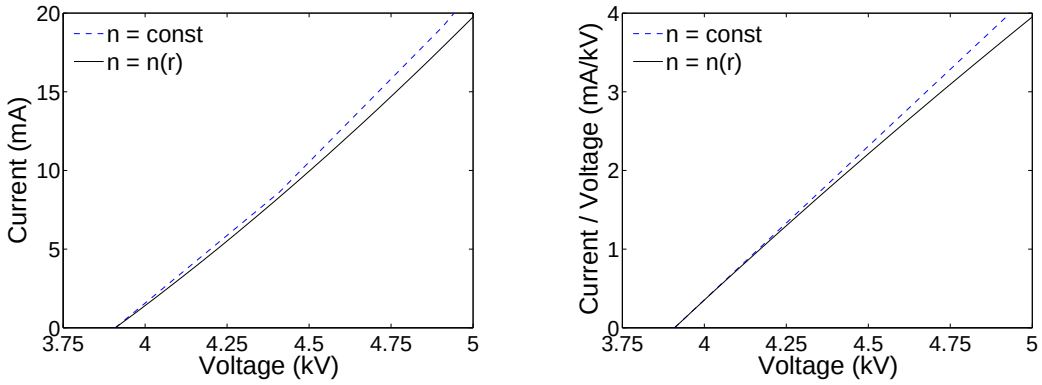

Figure 2.6. Current–voltage characteristics of stationary corona for $R_1 = 1$ cm and $R_2 = 1.1$ cm to show the convergence of the constant and variable ion density solutions at small currents.

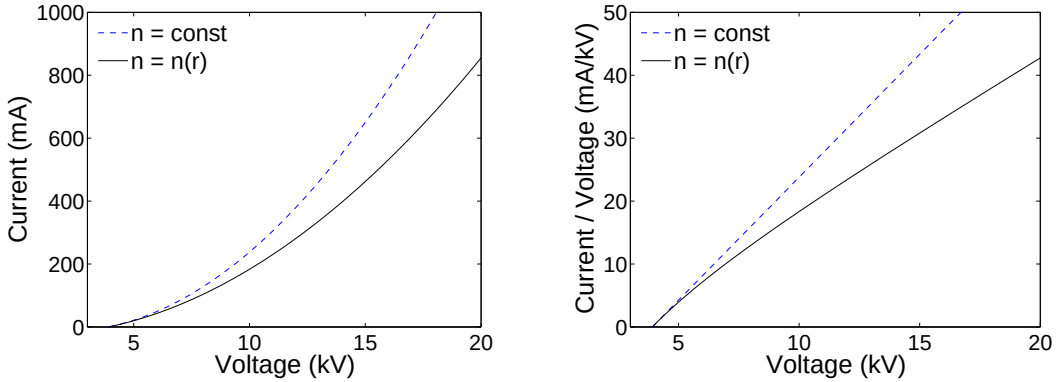

Figure 2.7. Current–voltage characteristics of stationary corona for $R_1 = 1$ cm and $R_2 = 1.1$ cm to show the divergence of the constant and variable ion density solutions at large currents.

this convergence for currents less than ~ 14 mA. In this case, the solutions are in reasonable agreement, with a difference typically less than 1 mA. The discussed limiting case represents one of the ways to validate the numerical voltage–current characteristic for the variable ion density model.

A general condition for the validity of the constant density model obtained from Equation (2.37), assuming $\Delta R = R_2 - R_1 << R_1$ and, therefore, representing R_2^3

in the form

$$R_2^3 = R_1^3 \left(1 + \frac{\Delta R}{R_1}\right)^3 \approx R_1^3 \left(1 + \frac{3\Delta R}{R_1}\right). \tag{2.42}$$

Having substituted the above expansion in Equation (2.37), we obtain an expression allowing direct evaluation of ΔR and I combinations for which the constant density assumption remains valid,

$$\Delta R I < 2\pi\varepsilon_0\mu_i E_c^2 R_1^2. \tag{2.43}$$

Chapter 3

Non-Stationary Corona and Upward Leader Model Formulation

Having established a stationary approach, the spherical model can now be developed for a non-stationary solution that can be used to simulate the initial conditions for the development of leaders from lightning rods of different radii. In the non-stationary solution, a transient ion density is defined as $n = n(r, t)$. Using a numerical approach, a non-stationary model is formulated, which can be further expanded to include in consideration streamer and leader processes (see Section 3.2).

3.1 Corona

As with the solution for a corona with stationary, radially dependent ion density, the exact solution for non-stationary corona cannot be found analytically. A derivation of the current–voltage relationship was not attempted. However, a solution for non-stationary corona was found using the electromagnetic equations to

follow with a numerical implementation. The simulation is discrete in both time, Δt, and space, Δr. The derivation that follows is based on the approaches and models discussed in, e.g., *Aleksandrov et al.* [2002]; *Aleksandrov et al.* [2005b]; and *Bazelyan et al.* [2008].

3.1.1 Finite-Difference Time-Domain Equations for Non-Stationary Corona Modeling

Similarly to stationary corona, when the electric field on the inner radius is less than the critical electric field for corona initiation, $E(R_1) < E_c$, there is no ion density, $n = 0$ m^{-3}. In this case, electric field and voltage are still defined by Equations (2.4) and (2.3). When the voltage on the inner electrode exceeds the critical voltage as defined by Equation (2.5), corona is initiated. For non-stationary corona $E(R_1, t) = E_c$ and $n = n(r, t)$.

In order to implement a numerical solution for non-stationary corona, equations for electric field and ion density must be established for discrete time and space. For electric field, Gauss's Law,

$$\oiint \vec{E} \cdot \, d\vec{S} = \frac{1}{\varepsilon_0} \iiint \rho \, dV, \tag{3.1}$$

was converted to a discrete domain, such that

$$E(r + \Delta r, t) = E(r, t) \frac{r^2}{(r + \Delta r)^2} + \frac{q_e n(r + \Delta r, t)}{\varepsilon_0} \frac{(r + \frac{\Delta r}{2})^2}{(r + \Delta r)^2} \Delta r. \tag{3.2}$$

In a similar way, the continuity equation,

$$\frac{\partial n_i}{\partial t} + \nabla \cdot (\mu_i n_i \vec{E}) = 0, \tag{3.3}$$

was converted for use in discrete coordinates for ion density.

$$q_e n(r, t + \Delta t) = q_e n(r, t) - \frac{1}{V^*} \left[F(r, t) - F(r - \Delta r, t) \right], \tag{3.4}$$

where V^* and flux, F, are defined as

$$V^*(r) = \frac{4\pi(r + \frac{\Delta r}{2})^2 \Delta r}{\Delta t}, \tag{3.5}$$

$$F(r, t) = 4\pi r^2 n(r, t) \mu E(r, t) q_e. \tag{3.6}$$

Flux, having units of amperes, is useful because it defines the current that flows through any given point in the system. Flux can be used to define current as it was defined in the stationary case. That is, the current into the system, $I(t)$, can be defined as

$$I(t) = F(R_1, t). \tag{3.7}$$

3.1.2 Numerical Approach

In order to deal with the dynamics of the non-stationary system, there must be a limit on Δt so that the numerical discretization scheme remains stable between time-steps. The particles in the system must not be permitted to pass between two discrete points in the time between steps [*Potter*, 1973, pp. 72–76]. That is, the distance that the ions travel during one time step must be less than the discrete length of space, or

$$\mu_i E_{\max} \Delta t \leq \Delta r. \tag{3.8}$$

Thus, the limit on the discrete steps in time is

$$\Delta t \leq \frac{\Delta r}{\mu_i E_{\max}}. \tag{3.9}$$

This is a modification of the Courant–Friedrichs–Lewy Condition [*Potter*, 1973, p. 72]. Since Equation (3.9) is dependent on the maximum electric field and the electric field varies with time, Δt must be calculated separately for each advancing step in time.

To implement this model, the simulation was driven by the voltage applied to the system, $U(t)$, defined such that $dU/dt \geq 0$. Corona is initiated when $E(R_1, t) > E_c$ in a corona-free system. The time of corona initiation, t_c, is defined when $E(R_1, t_c) = E_c$, where $E(r, t)$ is defined by Equation (2.4). In free space (when $n(r, t_c) = 0$ for all r) then $U(t_c) = U_c$, where U_c is defined in Equation (2.3).

At the time of corona initiation the electric field is known over the entire domain. Since

$$E(R_1, t_c) = E_c, \tag{3.10}$$

$E(r > R_1, t_c)$ can be calculated using Equation (3.2) at radius grid points, beginning at $r = R_1 + \Delta r$. Also, at the time of corona initiation, the ion density and flux are partially known. At the time right before t_c, the flux and ion density are zero at all grid points. At t_c, the ion density and flux could have changed only at the first grid point (i.e., directly on the sphere at R_1), therefore

$$n(r > R_1, t_c) = 0, \tag{3.11}$$

$$F(r > R_1, t_c) = 0. \tag{3.12}$$

For the next step in time, $t = t_c + \Delta t$, the current into the system must be determined to account for the increasing potential and to maintain the electric field on the surface of the inner electrode at a constant value of E_c. (The electric field at the inner electrode is always indirectly accounted for in the condition that $E(R_1, t) = E_c$ to find the necessary current.) To find this current, the ion density at the inner radius for the past time, $n(R_1, t_c)$, can be determined using a bisection method in order to satisfy the condition (mathematically equivalent to Equation (2.36)) that

$$U(t) = \int_{R_1}^{R_2} E(r, t)\, dr. \tag{3.13}$$

The bisection algorithm begins with a high (n_H), low(n_L), and middle (defined as: $(n_L + n_H)/2$) guess for $n(R_1, t_c)$. For each guess, $n(r > R_1, t_c + \Delta t)$ can be found and used to calculate $E(r > R_1, t_c + \Delta t)$. The error in calculating $U(t)$ (the boundary condition on the inner electrode) from the low, high, and middle guess by using Equation (3.13) is determined. If the error of the middle guess is below zero, then the middle guess becomes the new low guess. Likewise, if the error of the middle guess is greater than zero, then the middle guess becomes the new high guess. The process repeats until the error of the middle guess comes within the chosen error tolerance, ε (typically $\varepsilon = 10^{-3}\%$). The readers are referred to *Press et al.* [1992, pp. 117–119]] for details on the bisection search algorithm.

After the bisection process is complete, $E(r, t_c + \Delta t)$, $n(r > R_1, t_c + \Delta t)$, and $F(r > R_1, t_c + \Delta t)$ have been determined. The time of the system can be increased by Δt (calculated by Equation (3.9)). The voltage applied to the system at that time can be found through $U(t)$, which is defined uniquely for the simulation. For the current time and voltage, if $U(t) > U_c$, then the bisection process can be repeated for the next point in time in order to find the current being injected into

the system $I(t)$.

If, however, corona is no longer being initiated for this time and voltage (i.e., $U(t) < U_c$), $I(t) = 0$ A, and the ion density already in the system drifts as defined by flux. In this case, the potential at the grid points between the electrodes will be found using the Thomas algorithm with the known ion density and the boundary conditions that the potential at inner electrode is $U(t)$ and the potential at the outer electrode is 0 V [*Suli and Mayers*, 2003, pp. 93–98, and references therein]. Having found the potential at all grid points, the electric field can be found by the inverse of Equation (3.13),

$$E(r) = -\frac{\partial V(r,t)}{\partial r}. \tag{3.14}$$

This drift process repeats until $U(t) > U_c$, where corona is initiated and the computational cycle discussed above is repeated.

This process can be repeated indefinitely or until a defined condition through discrete steps in time, limited only by computational resources.

With a model of non-stationary corona, the development of streamers and leaders from the inner electrode can be traced. As explained in Section 1.1, an upward leader discharge is generated in two steps. First, the corona reaches a condition to ignite streamers (i.e., streamer corona). Second, the streamer channels merge and the resulting current becomes sufficient to form a thermalized leader channel. The following section explains the specific criteria for both of these processes.

3.2 Streamer Zone and Leader Initiation

By initiated upward streamers and leaders, a lightning rod will attract downward leaders propagating downward from a thundercloud above. In this way, a lightning

rod protects the surrounding area and structures from being hit by lightning. A measure of a lightning rod's strike-receptiveness can be found in the time that it takes for an upward leader to be initiated, t_L.

When a corona develops, there is an extremely thin ionization layer that forms on the tip of the electrode. This layer is assumed to provide infinite charge into the system while the corona matures. A streamer is formed when the ionization layer moves away from the surface of the electrode. When this happens, electrical breakdown occurs and streamers form [e.g., *Aleksandrov et al.*, 2002; *Cooray*, 2003, pp. 70–76]. The quantification of the movement of the ionization layer can be found through the Meek condition, which states that streamers form when

$$\int_0^d \alpha(E)\, dx > 18 \sim 20. \tag{3.15}$$

The distance, d, is the point where $\alpha[E(d)] \approx 0$ and α is defined as

$$\alpha(E) = \frac{\nu_i(E) - \nu_a(E)}{|\mu_e|}, \tag{3.16}$$

where ν_i is the ionization frequency, ν_a is the two-body dissociative attachment frequency, and μ_e is the electron mobility in air.

As an alternative approach, *Aleksandrov et al.* [2005a] noted that a simple analysis of the electric field could also determine if the ionization layer has developed beyond the surface of the inner electrode. If the electric field at any point beyond the tip is higher than the critical electric field that is maintained at the tip, E_c, then the condition is satisfied. In other words, streamers will form when

$$\left.\frac{\partial E}{\partial r}\right|_{r=R_1} > 0. \tag{3.17}$$

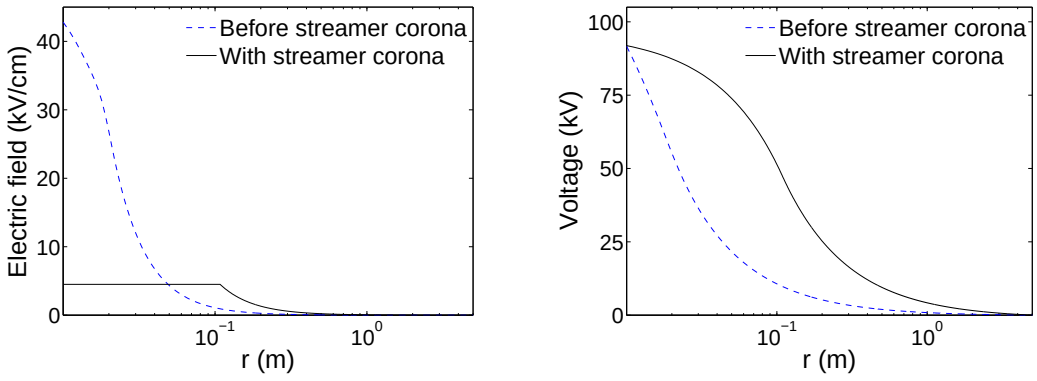

Figure 3.1. A generic illustration of the formation of a streamer corona showing (a) electric field and (b) voltage before and after the formation of streamers. The streamer corona region here has a length of 0.1 m.

It should be noted that this condition has not been tested or mathematically proven. However, the results of Section 4.2 indicate that this condition is nearly equivalent to the Meek condition given by Equation (3.15).

When the Meek condition is satisfied, a streamer corona forms. The electric field is taken to be 4.5 kV/cm along the length of the resultant streamer zone [*Raizer*, 1991, p. 355], and the ion density within the streamer corona is assumed to be determined by this electric field. The length of the streamer zone is restricted by the voltage boundary conditions of $U(t)$ and 0 V at the inner and outer electrodes, respectively. Illustrative plots of the electric field and voltage in the system during the transition from corona to streamer corona can be seen in Figure 3.1. In the model presented here, when a streamer corona forms, the length of the streamer zone is increased until the electric field throughout the domain satisfies the voltage present at the inner electrode. This analysis of the length of the streamer zone differs from previous models of streamers [*Aleksandrov et al.*, 2005a], where the length of the streamer zone was determined by the "spatial distribution" of the

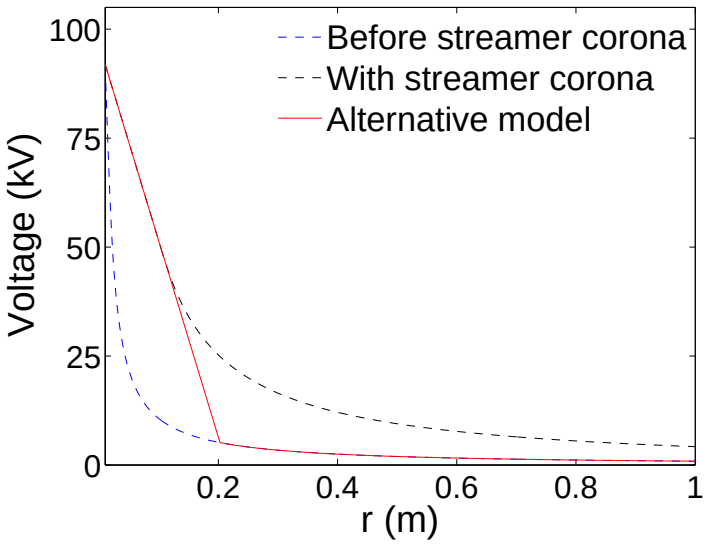

Figure 3.2. The generic formation of a streamer in regards to voltage, indicating the differences between the method used here and an alternative method [*Aleksandrov et al.*, 2005a]. The streamer here has a length of 0.1 m by the first method and a length of 0.2 m by the alternative method. (Simulation domain is 5 m).

voltage. This alternative model is illustrated in Figure 3.2. From this graph, it can be seen that the alternative model provides a sharp discontinuity in the derivative of voltage, which would cause an unrealistic electric field. This unrealistic electric field would not be equivalent to the electric field shown in Figure 3.1 and would be unable to satisfy the boundary conditions placed by the voltages at the electrodes and the ion density distribution required to maintain 4.5 kV/cm field in the streamer zone.

Once a streamer corona has been formed in this system, it is not sustained and the related deposited ion density begins to dissipate immediately. From this step, a rising voltage will cause a corona to form again when $E(R_1)$ rises to the value of E_c at the inner electrode surface. The corona and streamer process will repeat. If the voltage applied to the system has been consistently rising, the streamer length will increase with each new pulse of streamers and an assumption of quasi-continuous

propagation of the streamer zone may be justified.

Directly after streamers have been initiated, it is possible for the streamer zone to form into a leader. A large concentration of streamers at the inner electrode will cause heating in the area. When the temperature in atmosphere reaches $\approx 1500 - 2000$ K, electron detachment occurs from O_2^- ions in the plasma surrounding the tip [*Cooray*, 2003, p. 83]. This electron detachment is large enough that a leader forms in the system along the length of the streamer zone [*Raizer*, 1991, pp. 365–366].

Experiments at ground pressure have shown that leaders form when the length of the streamer corona is ≈ 1 m [*Raizer*, 1991, p. 366]. Due to the consistent electric field of ≈ 4.5 kV/cm along a streamer zone, this parameter can also be specified as an approximate 400-kV voltage drop along the length of the streamer zone [*Aleksandrov et al.*, 2005a]. In our model, we assume that a leader will follow this condition and be formed when

$$\Delta U_{\text{st}} > 400 \text{ kV}, \tag{3.18}$$

where ΔU_{st} is the change in voltage from the inner electrode to the outer edge of a streamer zone which has formed. The time of leader initiation, t_L is recorded at the point in time when Equation (3.18) is satisfied along a newly formed streamer zone.

Chapter 4

Non-Stationary Model Application

In this chapter, the model that was formulated in Chapter 3 is used to demonstrate non-stationary corona and lightning leader initiation for the one-dimensional spherical system.

4.1 Non-Stationary Corona Validation

To verify the non-stationary corona model, it was run using the same conditions as in *Aleksandrov et al.* [2002; 2005b]. Under these conditions, $U(t)$ was defined as

$$U(t) = \begin{cases} \dfrac{U_{\max}}{\tau}\, t & \text{if } t < \tau, \\ U_{\max} & \text{if } t \geq \tau. \end{cases} \tag{4.1}$$

For this instance, the corona will reach a steady-state solution. In the model, $R_1 = 1$ cm, $R_2 = 5$ m, and $U_{\max} = 300$ kV. The value of τ was varied as indicated. In the general model, $\Delta r = R_1/10 = 1$ mm and $\epsilon = 10^{-3}\%$ (variations will be noted).

A comparison of results from our model to the those presented by *Aleksandrov*

et al. [2005b] is shown in Figure 4.1 and clearly indicates the excellent agreement between the two models. For $\tau = 10^{-3}$ s, the current peaks at 3.4 mA and for $\tau = 10^{-3}$ s, the current peaks at a significantly lower value of 0.87 mA. The steady-state current solutions for both τ is about $I_{\text{ss}} = 0.068$ mA.

The differences between results presented in Figures 4.1(a) and 4.1(b) are likely due to the discretization of the system in time and space. The parameters Δr and Δt greatly affect the accuracy of the numerical solution. A slight change in Δr can drastically change the value found for U_c (by Equation (2.5)) and, consequently, the current in the system. The Δt parameter does not have a pronounced effect on the system unless it violates the criterion of Equation (3.9). Also, the error associated with the bisection process, ϵ, will affect the accuracy of the solution. Because of this, ϵ is kept at low values ($10^{-3}\%$). The values of the parameters discussed above (or, equivalent error values associated with the model) used by *Aleksandrov et al.* [2002] are unknown.

The non-stationary solution can also be verified through comparison of the steady-state regime and the stationary solution found in Section 2.1.2. Figure 4.2 shows the development of the non-stationary solution through time. For comparison with results from Section 2.2, here $R_1 = 1$ cm, $R_2 = 50$ cm, and $\tau = 10^{-2}$ s. From these figures, it is clear that the peak current occurs when $t = \tau$ and the voltage has reached $U_{\max} = 300$ kV. From this point in time, the current quickly settles into the steady-state solution, $I_{\text{ss}} = 1.50$ mA, which is in excellent agreement with current $I \approx 1.5$ mA at $V = 300$ kV for the stationary corona results shown in Figure 2.1.

The solutions in Figure 4.1(a) and Figure 4.2 also show the effect of outer electrode radius on the steady-state solution. For $R_2 = 5$ m, $I_{\text{ss}} = 0.07$ mA (from Figure 4.1(a), and for $R_2 = 50$ cm, $I_{\text{ss}} = 1.5$ mA (from Figure 4.2). That is, a

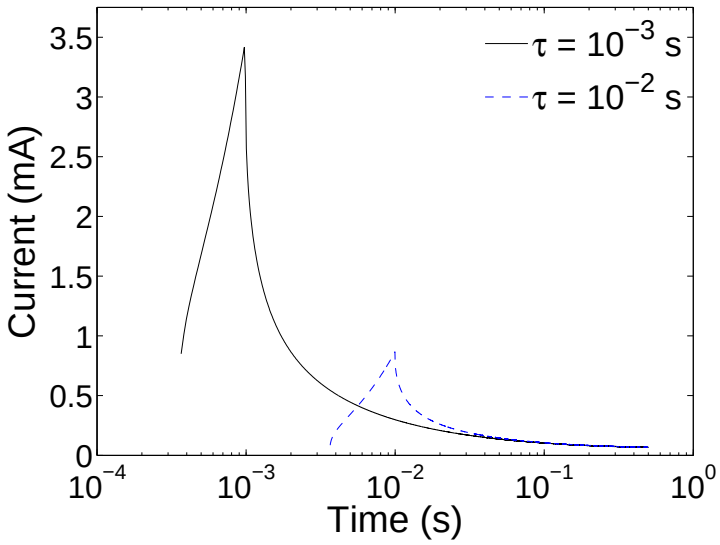

(a)

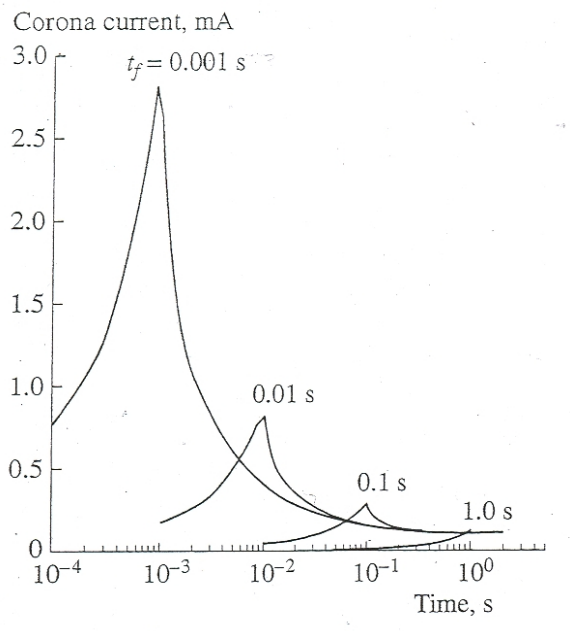

(b)

Figure 4.1. The current development of non-stationary corona for $R_1 = 1$ cm and $R_2 = 5$ m for (a) the non-stationary model developed in this thesis and (b) a model developed by *Aleksandrov et al.* [2005b].

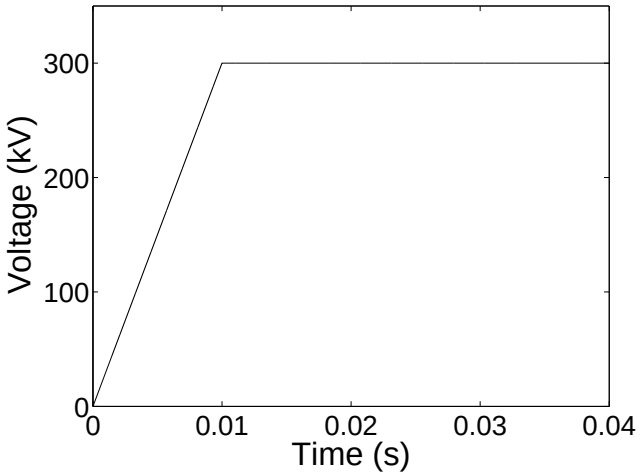

(a)

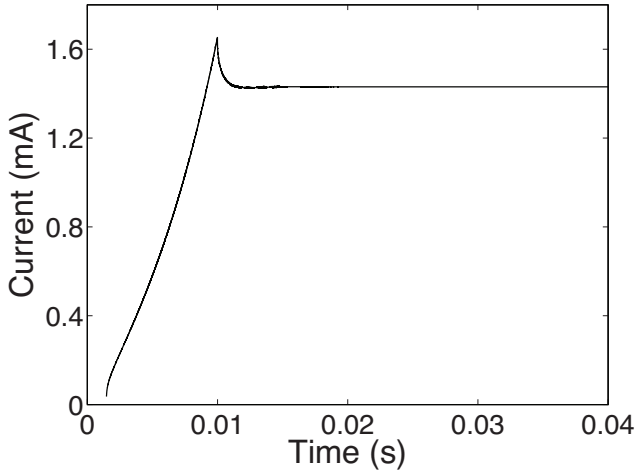

(b)

Figure 4.2. Applied voltage and current vs. time for numerically calculated non-stationary corona. The model parameters are: $R_1 = 1$ cm, $R_2 = 50$ cm, $\Delta r = 1$ mm, and $\tau = 10^{-2}$ s.

factor-of-10 decrease in R_2 leads to a factor-of-20 increase in steady-state current, $I_{\rm ss}$. Considering that, in the simulation of lightning rods with results shown in Section 4.2, the outer electrode is meant to be placed far enough away so that the solution appears as if $R_2 = \infty$, this places a restriction on how much R_2 can be

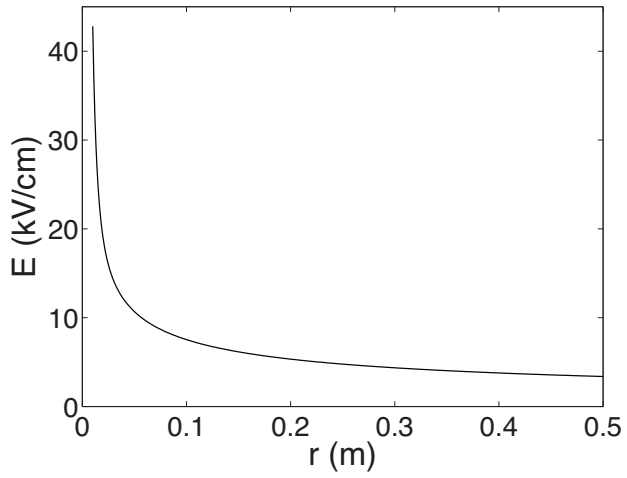

(a)

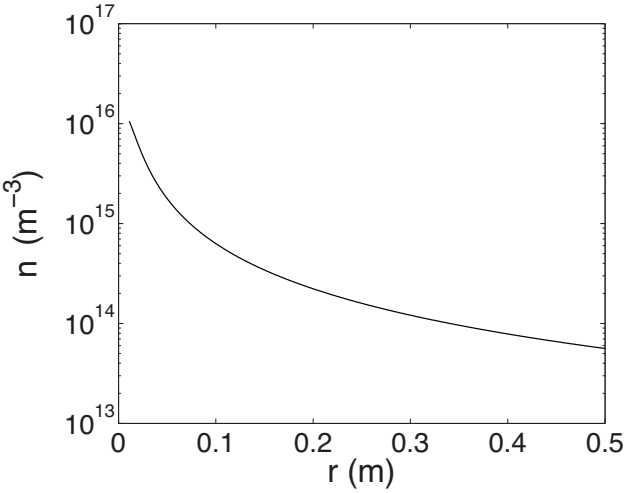

(b)

Figure 4.3. The steady-state solutions for $E(r,t)$ and $n(r,t)$ taken at $t = 0.04$ s for model parameters $R_1 = 1$ cm, $R_2 = 50$ cm, $\Delta r = 1$ mm, and $\tau = 10^{-2}$ s.

decreased and still keep the model accurate. Because of this clear restriction, R_2 will be taken at 5 m for Section 4.2. This radius will be large enough to deal with the dynamic voltage presented there without reaching steady-state.

In addition, the steady-state solutions for the electric field and ion density can be seen in Figure 4.3. These are comparable to the stationary solutions seen in

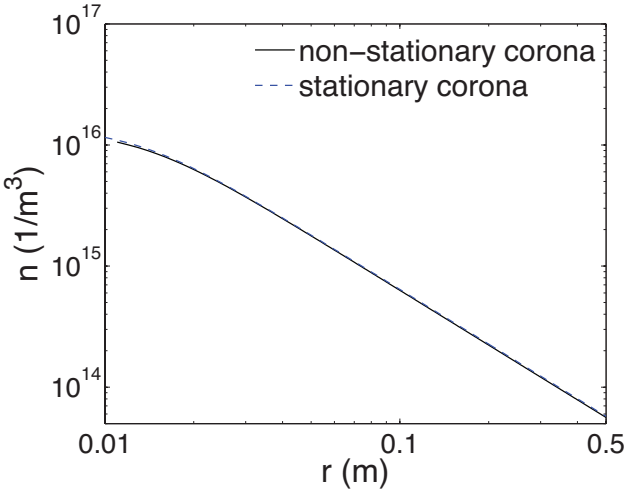

Figure 4.4. A comparison of the steady-state solution for $n(r,t)$ taken at $t = 0.04$ s and the stationary solution for $n(r)$. In both graphs, $I = 1.50$ mA. In the simulation, $R_1 = 1$ cm, $R_2 = 50$ cm, $\Delta r = 1$ mm, and $\tau = 10^{-2}$ s.

Figure 2.2. Ion density is concentrated around the inner electrode and decays by nearly two orders of magnitude toward the outer electrode. The electric field follows the same trend. An exact match in the stationary analysis is not seen because, in this instance, the steady-state current ($I_{\text{ss}} = 1.50$ mA) is too small for the range of the stationary graphs shown in Figure 2.2. However, by knowing the steady-state current, an appropriate stationary solution can be found for comparison. With a steady-state current of $I_{\text{ss}} = 1.5$ mA, the appropriate ion density curve can be compared to the steady-state ion density. Figure 4.4 shows this comparison between stationary and non-stationary steady-state for ion density. The steady-state curve is the same data as in Figure 4.3(b), and the stationary curve is calculated using the variable density stationary model of Chapter 2 for $I = 1.50$ mA. In comparing the graphs, there is less than 4% error, defined as

$$\frac{|n_{\text{non-stationary}} - n_{\text{stationary}}|}{n_{\text{non-stationary}}} < 4\%. \tag{4.2}$$

The correlation of these curves indicates that the steady-state solution is correct.

4.2 Initiation of Upward Leader

With the non-stationary corona model validated, upward leaders can be simulated in the system using the criteria for streamer and leader initiation described in Section 3.2.

At this point in discussing the model, it will be beneficial to think in terms of physical mechanisms. With that in mind, the inner electrode will now be referred to as the tip of a lightning rod, with the inner electrode radius representing the rod radius. The voltage applied to the tip of the rod occurs because of the effects of the charge growth in a thundercloud or the effects of an approaching downward leader.

For the first upward leader simulation, the voltage applied to the system is defined for all time as

$$U(t) = \frac{U_0}{\tau} t. \tag{4.3}$$

The voltage plateau used in Equation (4.1) has been eliminated because the dynamic leader and streamer initiations will only occur when the voltage is transient and rising: $dU/dt > 0$. When the only goal is to initiate streamers and leaders, the plateau at $U_{\max}$ unnecessarily complicates the situation. In a natural occurance, the rise time, τ, would be due to an approaching downward leader. With this in mind, τ should be kept in the millisecond range, as indicated by previous experiments [*Moore et al.*, 2000a; *Moore et al.*, 2003]. For comparison's sake, U_0 is kept at 300 kV [*Bazelyan et al.*, 2008].

Using these input parameters, a movie was created from a time-dependent

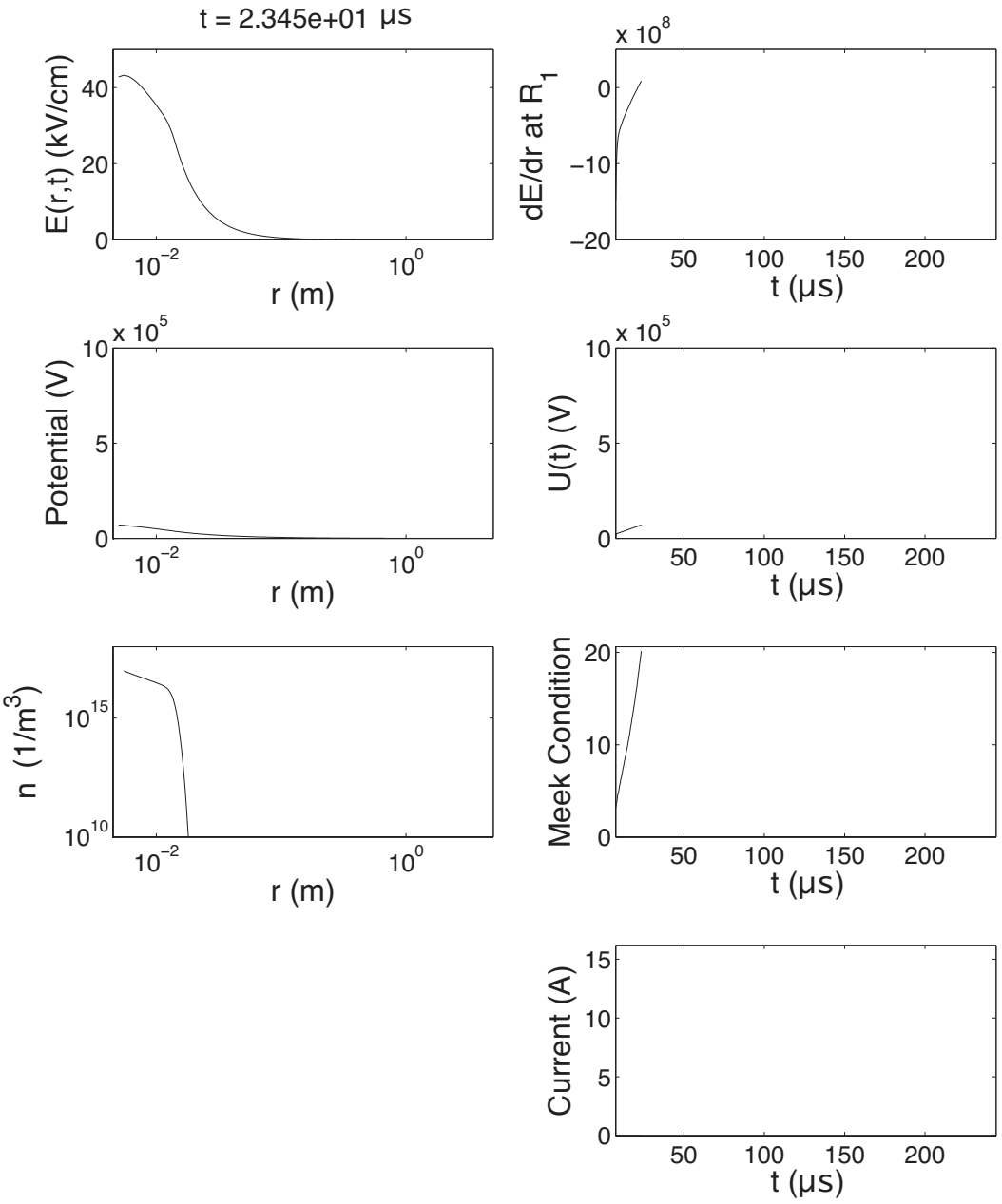

Figure 4.5. The physical parameters of the model at $t = 23.45$ μs, just before the first streamer initiation, for the model case with $R_1 = 5$ cm, $R_2 = 5$ m, and $\tau = 10^{-4}$ s.

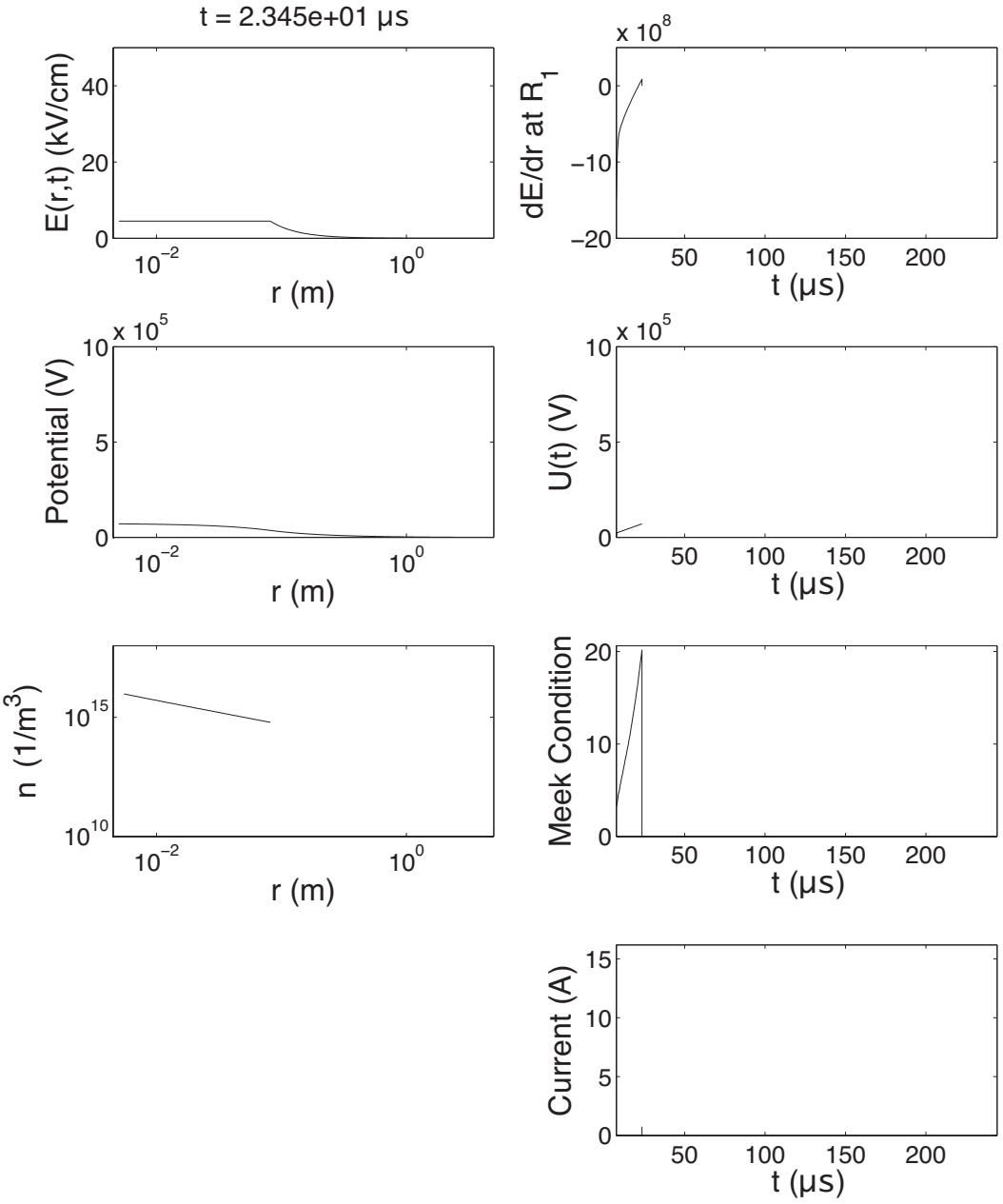

Figure 4.6. The physical parameters of the model at $t = 23.45$ μs, just after the first streamer initiation, for the model case with $R_1 = 5$ cm, $R_2 = 5$ m, and $\tau = 10^{-4}$ s.

simulation to explore the non-stationary effects of the corona and the streamer and leader initiations (see Section A.1). The simulation was run using the Meek condition for streamer initiation, $R_1 = 5$ mm, $R_2 = 5$ m, and $\tau = 100$ μs. The rise time used in this example is too short for practical application, but efficiently demonstrates the performance of the model.

Figures 4.5 to 4.8 document several representative instants of time during model execution. On the left side, the figures display the electric field, potential, and ion density between the lightning rod and the end of the simulation domain for a certain, indicated time. The plotted quantities are shown vs. $\log_{10}(r)$ to emphasize variations near the inner electrode. On the right side, the figures show the time development of $\partial E/\partial r$ at R_1 (see Equation (3.17) and related discussion), the voltage applied to the rod, the Meek condition (as defined by Equation (3.15)), and the current from the rod into the system.

The model begins with the development of corona around the tip of the rod. Figure 4.5 shows the parameters of the simulation at $t = 23$ μs, just before the first streamer corona is initiated. At this point, the voltage is relatively low, $U(t) \approx 70$ kV. Although corona has been initiated, there is negligible current in the system. At this point, the good correlation of the Meek condition and $\partial E/\partial r$ at the rod, R_1, can be seen. The Meek condition is satisfied at this point in time, while the later condition was satisfied at 21.51 μs, corresponding to only an 8% difference between the two times. Therefore, either condition could be used for streamer corona initiation and Equation (3.17) is validated.

The first streamer corona initiation in the simulation is shown in Figure 4.6. At this point, the electric field is reduced to 4.5 kV/cm to satisfy the streamer corona condition. The streamer zone length is determined by the boundary conditions imposed by the voltage. In this case, the length of the streamer zone is 8 cm and

it has a voltage drop along its length of 34.4 kV. The streamer zone distributes an ion density in the system on the order of 10^{15} m^{-3} along its length. The current that this distribution causes (though barely visible in the figure) is 0.7 A.

Figure 4.7 shows the point in time midway between the first and second streamer corona initiation. At this point, the voltage applied to the rod has risen to ∼91 kV and the electric field at the rod has reached the critical voltage for corona initiation, $E_c = 43$ kV/cm. The ion density being injected into the system can be seen merging with the ion density that was distributed by the first streamer corona.

A leader is initiated at the end of the simulation, and this point is shown in Figure 4.8. This occurs at $t = 244$ μs, with an applied voltage of 732 kV. The streamer corona that has formed has a length of 90 cm and injects a current of 16 A into the system. The voltage along its length is $\Delta U_{\text{st}} \approx 400$ kV. In this case, ΔU_{st} satisfies the condition for leader initiation specified in Equation (3.18) and a leader will be formed in the system at this point. The simulation run is stopped when criterion for leader initiation is satisfied.

This final figure of the simulation shows how the bursts of streamer corona form as the voltage rises. Each sharp peek in current corresponds to a new streamer corona initiation. Each streamer zone formed is slightly longer than the previous one, as seen through the larger current injected into the system. In addition, the voltage drop along the streamer zone grows with each streamer corona burst. This increase in current, length and ΔU_{st} is due to the rising applied voltage on the rod, $U(t)$: a larger applied voltage is able to support a longer streamer zone. When the streamer reaches nearly 1 m (0.8 m) (as seen in Figure 4.8, ΔU_{st} has increased to be greater than 400 kV and a leader is initiated.

The pulsing effect on the current through a lightning rod qualitatiively matches observations by *Moore et al.* [2000a; 2000b; 2003]. In these studies, when lightning

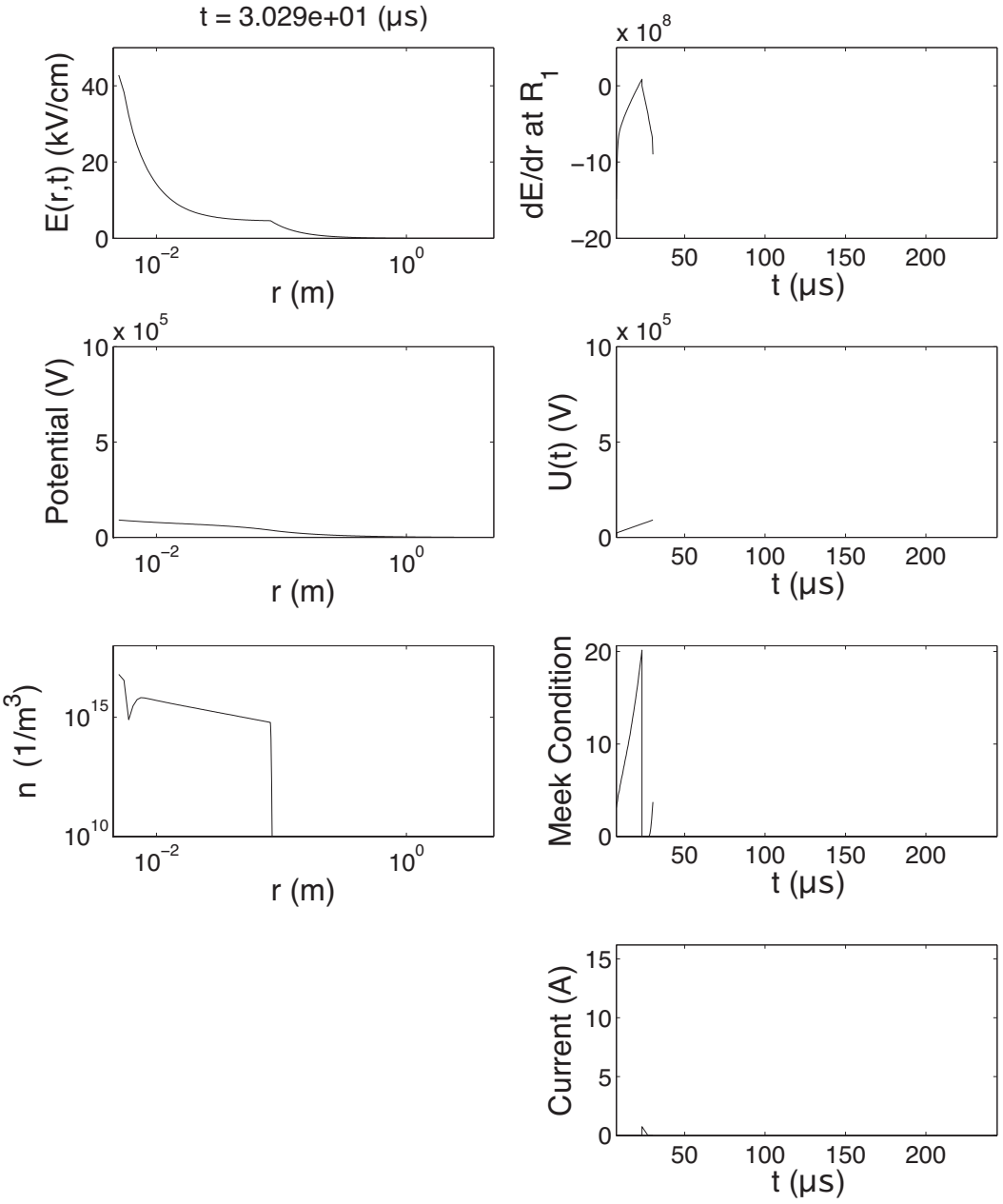

Figure 4.7. The physical parameters of the model at $t = 30.29$ μs, midway between first and second streamer initiations, for the model case with $R_1 = 5$ cm, $R_2 = 5$ m, and $\tau = 10^{-4}$ s.

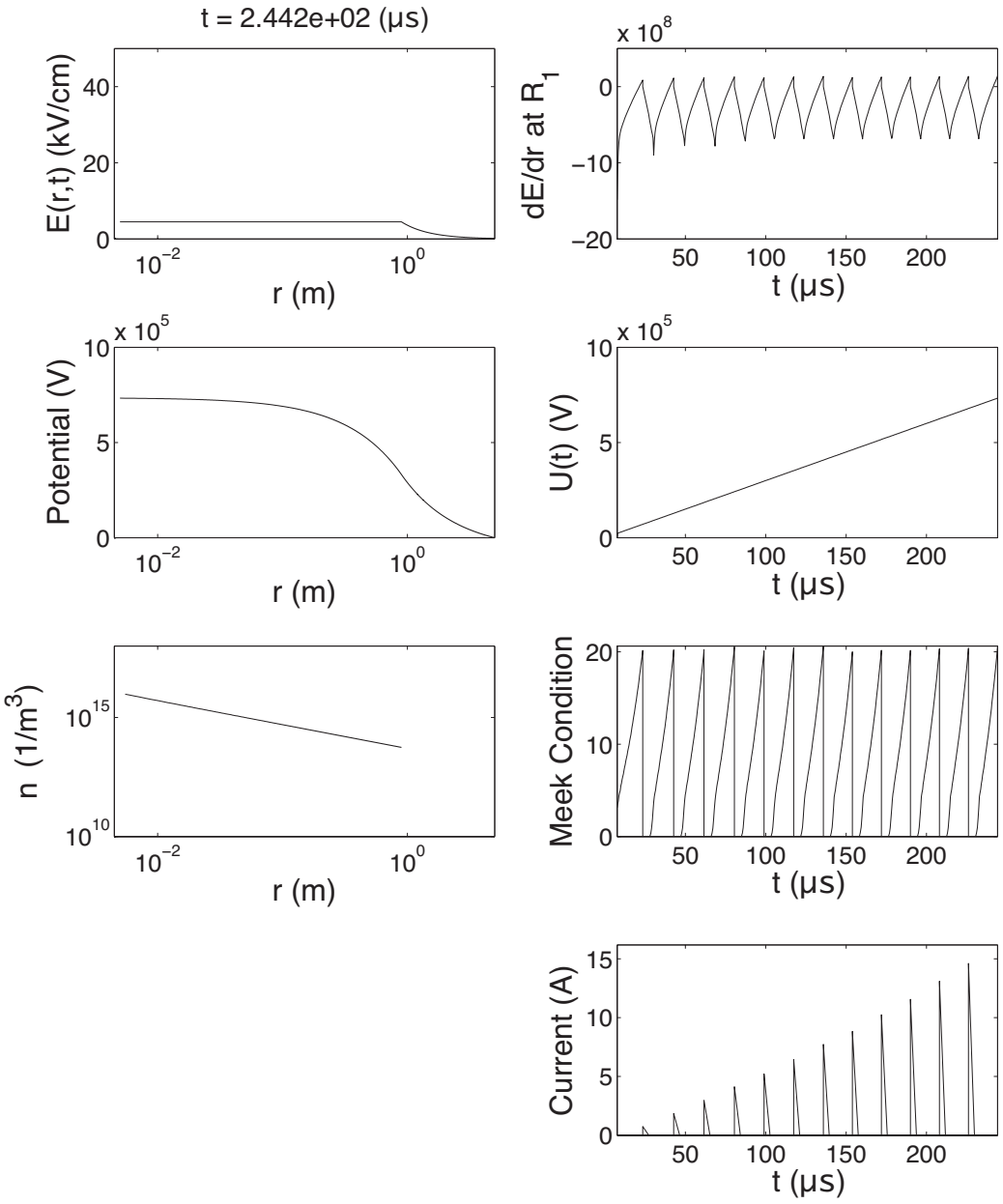

Figure 4.8. The physical parameters of the model at $t = 244.2$ μs, showing the streamer initiation which will lead to a leader, for the model case with $R_1 = 5$ cm, $R_2 = 5$ m, and $\tau = 10^{-4}$ s.

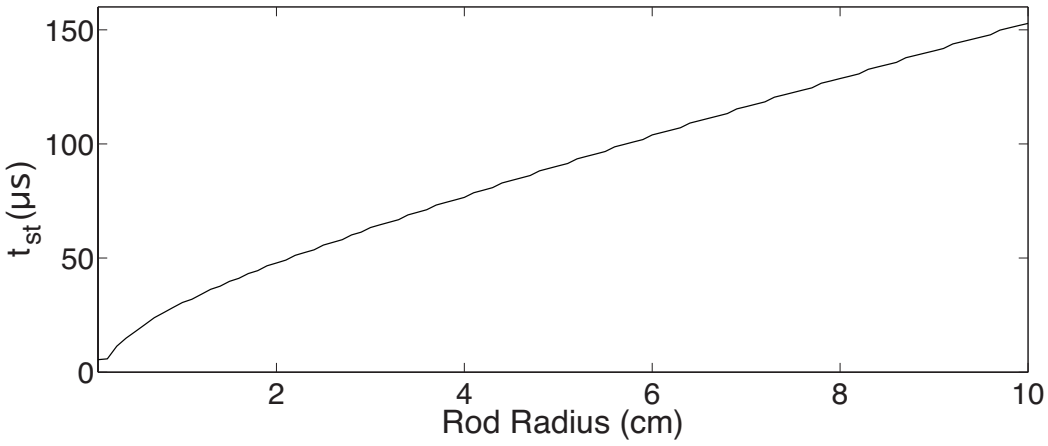

Figure 4.9. Time of first streamer corona initiation, t_{st}, vs. rod radius, R_1, for a constantly rising voltage. Model parameters are: $R_2 = 5$ m, and $\tau = 10^{-4}$ s.

strikes a lightning rod (or the surrounding area), a current is seen through the rod, which grows as the downward leader approaches. The currents reported are comparable to the 16-A current seen in the leader initiation shown in Figure 4.8. Specifically, *Moore et al.* [2000b] reports field study data for strikes near lightning rods that show an increasing, pulsing current that ranges from 0 to 8 A (the equipment saturated at 8 A).

Having established that the model, as described by Figures 4.5 to 4.8, is accurate, the model was run for a range of rod radii and rise times. Figures 4.9 to 4.12 show the results for these simulations.

The time of initiation for the first streamer corona, $t_{\rm st}$, vs. rod radius is shown in Figure 4.9 for a voltage rise time of $\tau = 100$ μs. Again, as discussed previously, this small rise time is being used for demonstration purposes, as the effects of streamer and leader initiation are more pronounced over a larger range of radii for faster rise times. Here, it is evident that larger radii have longer time for streamer corona inititation: for $R_1 = 1$ mm, $t_{\rm st} = 5.5$ μs; for $R_1 = 10$ cm, $t_{\rm st} = 153$ μs.

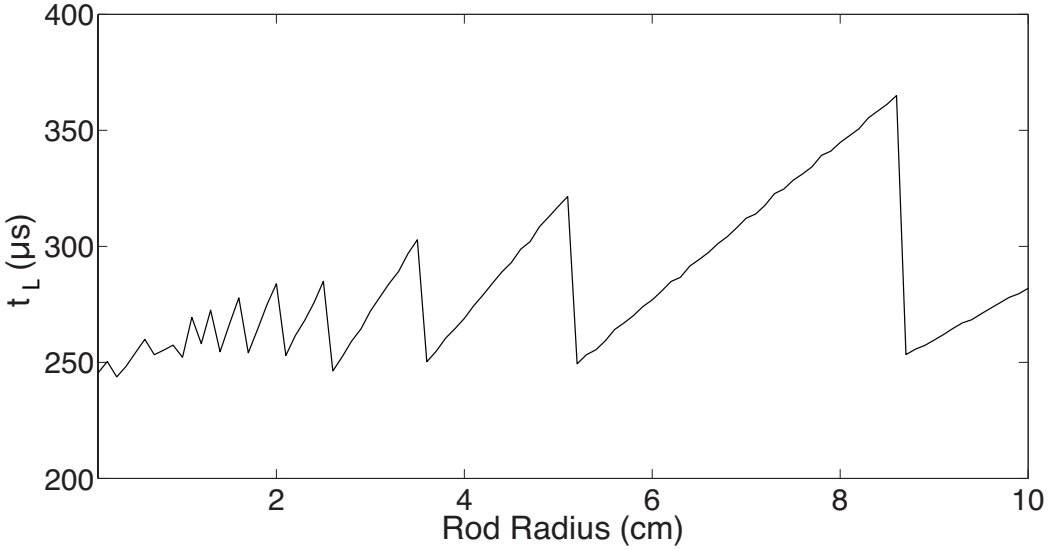

Figure 4.10. Time of leader initiation, t_L, vs. rod radius, R_1, for a constantly rising voltage. Model parameters are: $R_2 = 5$ m, and $\tau = 10^{-4}$ s.

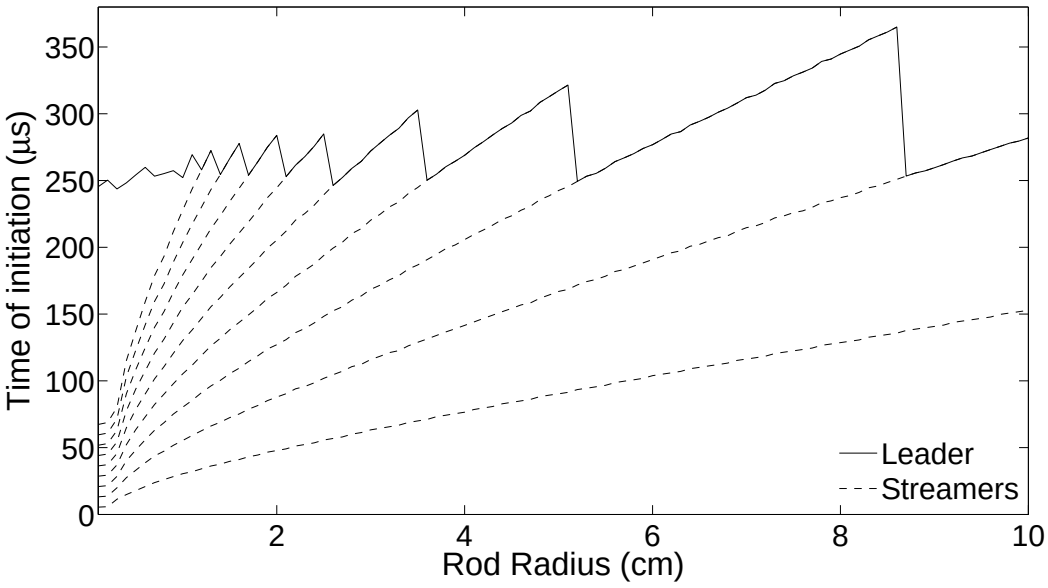

Figure 4.11. Superposition of Figures 4.9 and 4.10 with time of second–ninth streamer corona initiation to show the correlation between the initiation of streamers and leaders. Model parameters are: $R_2 = 5$ m, and $\tau = 10^{-4}$ s.

Since a smaller radius has a lower critical voltage for corona ignition, U_c (as defined by Equations (1.1) and (2.5)) and a sharper peak in electric field at the tip of the rod, it is clear that the Meek condition, which depends on the electric field near the tip, would be satisfied in a shorter amount of time for smaller rod radii.

Alternatively, leader initiation does not show this consistent trend between rod radii and time of initiation. Shown in Figure 4.10, the time of leader initiation, t_L, oscillates with the change in rod radii, remaining consistently in the area of $t_L \approx 250$ μs.

In order to understand the oscillation in Figure 4.10, the dynamics between times of streamer corona and time of leader initiation were explored. Superimposing Figure 4.9 onto Figure 4.10 and adding the time of initiation for the second through ninth streamer coronas, a clear relationship can be seen in Figure 4.11. Here, it is clear that the oscillation occurs because a leader can only be initiated immediately after a streamer has been formed. For example, with a rod radius of 4 cm, the first streamer burst is formed at 80 μs, the second at 140 μs, and the third at 200 μs. All of these streamer bursts have ΔU_{st} less than 400 kV, so a leader does not form. The fourth streamer burst, initiated at 270 μs, forms a leader because ΔU_{st} is greater than 400 kV. By comparison, a rod with a radius of 8 cm initiates 2 streamer bursts with $\Delta U_{\text{st}} < 400$ kV. The third streamer burst, at $t = 340$ μs, has $\Delta U_{\text{st}} = 585$ kV and initiates a leader.

With this example in mind, it is clear that the applied voltage, $U(t)$, becomes large enough to support a leader at 250 μs. However, there is a small delay in leader initiation because a streamer must be formed after this time. At this time (250 μs), the voltage applied to the inner electrode (750 kV) is strong enough to support a streamer zone with a 400-kV voltage drop along its length as described in Section 3.2. From Figure 4.11, it can be extrapolated that at extremely large

radii (around 20 cm), the first streamer initiated will also cause leader initiation. This means that large radii will suffer a delay in t_L because of the prolonged time that it takes for the first streamer to form.

The effect of rod radii on leader initiation for a constantly rising voltage, $U(t)$, is established for a range of rise times in Figure 4.12. The data from Figure 4.10 is shown as the smallest rise time on the graph. The relative importance of the oscillations seen for a rise time of 100 μs is small for a given rod radius. Due to the dynamics of the system, the minimum t_L rises linearly with respect to increasing rise time. This happens because a larger rise time will mean that it takes longer for the applied voltage to reach the point where it can support the voltage drop on a streamer zone necessary for leader formation.

In addition to the overall increase in t_L, it can be seen that, as the voltage rise time becomes longer, the rod radius has a larger affect on the time of leader initiation. To illustrate this point, Figure 4.13 shows the time of leader initiation,

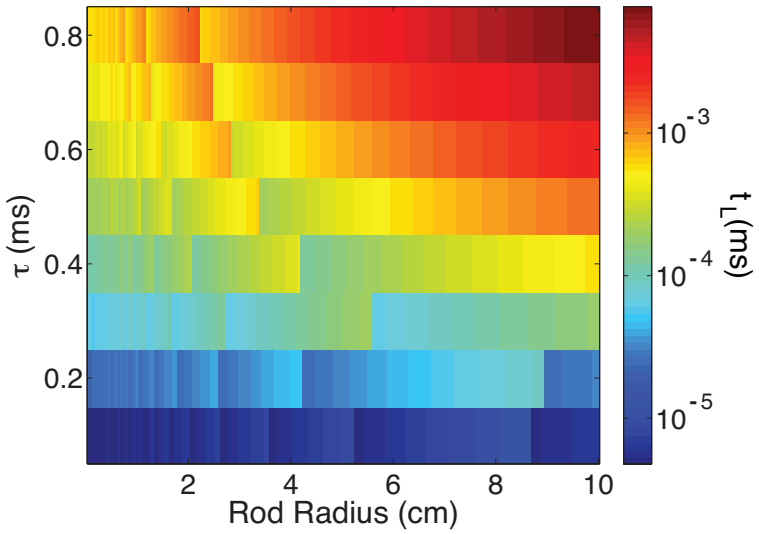

Figure 4.12. A color scale image of the leader initiation time, t_L, as a a function of voltage rise time, τ, and rod radius, R_1. In the model, $R_2 = 5$ m.

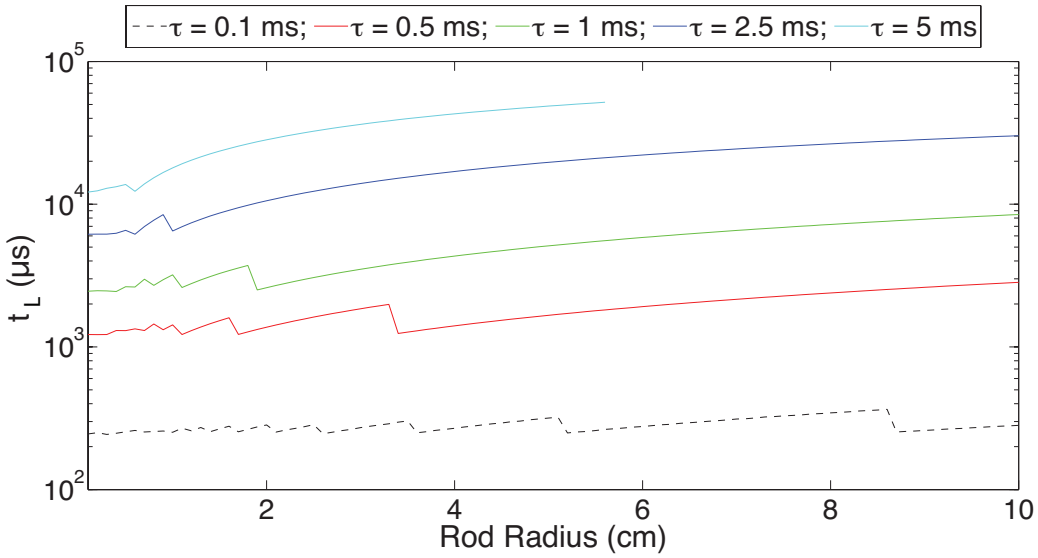

Figure 4.13. Time of leader initiation, t_L, vs. rod radius, R_1, for a several different voltage rise times. In the model, $R_2 = 5$ m.

t_L, for many different voltage rise times, τ. For a rise time of 0.1 ms (the same plot as in Figure 4.10), there is little variation in t_L and the leader is initiated by the second streamer corona for a rod radius of 10 cm. For this rise time, the rod radius has little effect on the time of leader initiation. A comparatively longer rise time of 5 ms gives an order-of-magnitude variation in t_L for the range of rod radii shown in Figure 4.13. This rise time also initiates a leader at the time of the first streamer corona for rod radii greater than 5 mm. At this rise time, a rod radius greater than $\sim$ 1 cm would be undesirable as it would have a longer time for leader initiation than rod radii less than 1 cm.

The same argument can be applied to any rise time. Generally, a rod radii that initiates a leader at the time of the first streamer corona is undesirable, as it will have a comparatively longer time of leader initiation, t_L, than rod radii that initiate streamers at the time of later streamer coronas.

Chapter 5

Conclusions

5.1 Scientific Contributions

A numerical model of spatially dependent ion density, stationary corona has been developed. As shown in Figures 2.1 and 2.7, this numerical model provides the current–voltage characteristic solution for a stationary corona. This solution is also validated in the limit as R_1 approaches R_2 for small currents, as seen in Figure 2.6, where the variable ion density solution approaches the simplified analytical solution for constant ion density. An analytical, closed form solution of spatially dependent, stationary corona is not known and for this reason the related solutions are not provided in the existing literature [e.g., *Roth*, 1995, pp. 256–260; *Aleksandrov et al.*, 2002; *Becerra et al.*, 2007; and others]. In using a numerical approach, the stationary corona current–voltage characteristic can be understood and quantified. The related solution represents one of the original contributions of this thesis.

A numerical solution for non-stationary corona has also been obtained. Though similar numerical solution has already been established [*Aleksandrov et al.*, 2002; *Aleksandrov et al.*, 2005a; *Aleksandrov et al.*, 2005b; *Becerra et al.*, 2007; *Bazelyan*

et al., 2008], the approach to the numerical solution is presented here fully with new modeling of the streamer corona regime and leader initiation. In addition, validation of the non-stationary model has also been presented. As the non-stationary corona solution reaches the steady-state regime, it converges to the solution for stationary, spatially dependent corona, as shown in Figure 4.4.

In regards to non-stationary upward leader initiation, a time-dynamic approach is demonstrated in this thesis. Similar to the upward leader discussion of *Bazelyan et al.* [2008] and *Aleksandrov et al.* [2005a], the model presented in this thesis simulates the initiation of streamers and leaders in the context of the time dynamics of non-stationary corona. The model progression of Figures 4.5 to 4.8 (see also Appendix A.1.) shows the development of streamer bursts through time. This progression is consistent with the current pulsing observed experimentally by *Moore et al.* [2000a; 2003].

In addition, the non-stationary corona and lightning model can be used to understand the role of a lightning rod's radius on the time of leader initiation. From the results given for a consistently rising voltage in Figure 4.12, it is clear that large radii have a distinctly higher time of leader initiation, particularly when larger (more realistic) rise times are explored. This inhibition on leader development gives larger radii (conservatively estimated for $R_1 > 5$ cm) a distinct disadvantage to intercepting an approaching downward leader. Therefore, any optimum lightning rod tip radius should be smaller than 5 cm, and likely in the range of 0–2 cm. In this thesis, only one case of the functional dependence of applied voltage on time, $U(t)$, was researched. It is highly plausible that other definitions of $U(t)$ may reveal a different relationship between rod radii and time of leader initiation.

5.2 Future Research

It is possible that investigations into the shielding effect could establish a lower limit for an optimum lightning rod tip radius. The shielding effect occurs when charge density in the atmosphere (which has been placed there through corona ignition and streamer formation) shields the lightning rod tip from the effects of voltage and electric field [*Bazelyan et al.*, 2008]. This layer of charge prevents the electric field at the tip of the rod from reaching E_c and initiating more corona and subsequent streamers into the system. In addition, the shielding effect limits the length of streamers that form in the system because of the voltage drop along the corona-shield. Many studies list the shielding effect as a reason why corona prevents leader initiation [*Bazelyan et al.*, 2008; *Aleksandrov et al.*, 2005b; *Becerra et al.*, 2007; *Becerra and Cooray*, 2006b].

Artificially, the shielding effect can be seen by inserting a spherical shell, or "wall", of ions into the system. By inserting this wall of ions, the voltage drop and electric field that forms along the wall alleviates the electric field seen at the tip of the electrode. Therefore, a higher applied voltage is necessary in order for E_c to be reached. Figure 5.1 shows the electric field and voltage of the simulation domain at the time of corona initiation for the same parameters as used in Figures 4.5 to 4.8 and in Appendix A.1. The movie of lightning development when a wall of ions is inserted can be found in Appendix A.2. Though these simulations appear to be the same, the wall of ions delays the start of corona initiation to 670 μs. Whereas, without the wall of ions, corona was initiated at 7.5 μs. The overall delay in the simulation occurs because it takes a longer time for the applied voltage on the rod tip to reach the necessary voltage for $E(R_1, t) = E_c$. This simulation demonstrates that a large amount of ions inserted into the system (essentially, the shielding

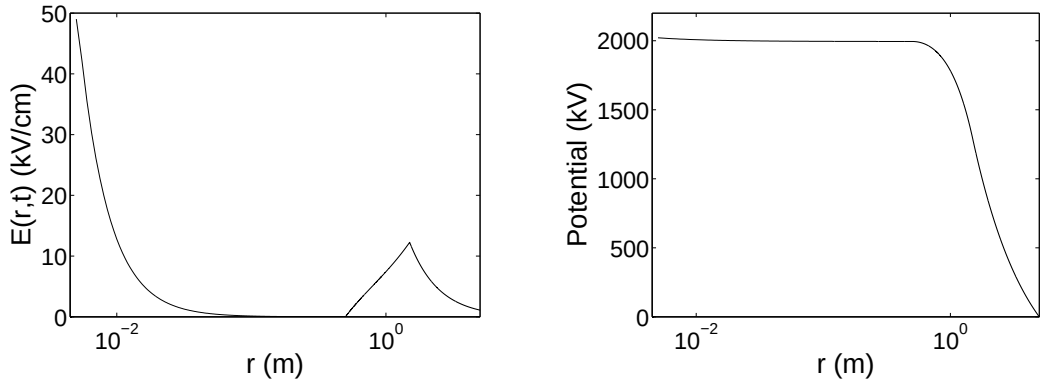

(a) (b)

Figure 5.1. The effect of a wall of ions on the (a) electric field and (b) voltage shown for a non-stationary lightning simulation at $t = 673$ μs. Model parameters are: $R_1 = 5$ cm, $R_2 = 2.5$ m, and $\tau = 10^{-4}$ s.

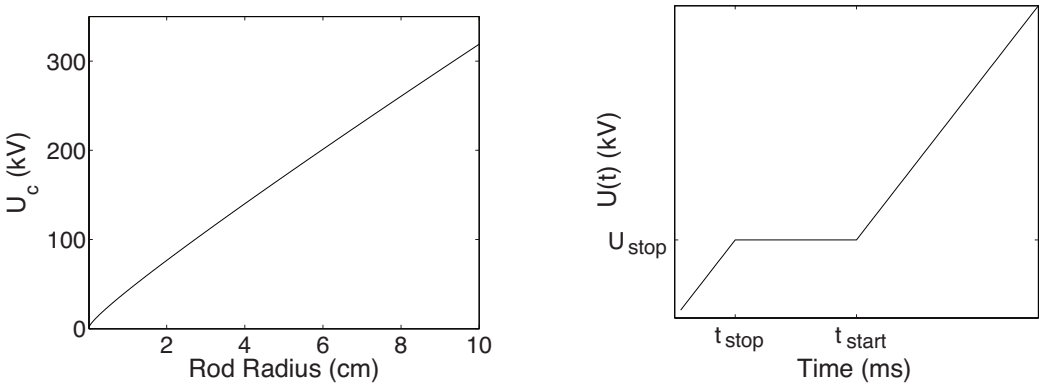

(a) (b)

Figure 5.2. (a) The critical voltage for corona initiation in free space, as calculated with Equations (2.5) and (1.1), compared to (b) the proposed voltage for simulating shielding effects.

effect) prevents corona, streamers, and leaders from forming and, overall, delays the time of leader initiation.

It is suggested that the delay in leader initiation due to the shielding effect is dependent on rod radius because, for smaller rod radii, the shielding effect occurs

more readily and at lower applied voltages. Figure 5.2(a) shows the relationship between critical voltage (for initiation of corona) and rod radii. A smaller radii will have a lower U_c for free-space. If a voltage like the one shown in Figure 5.2(b) were to be applied to the rod, any radii with $U_c < U_{\text{stop}}$ would initiate corona (and possibly streamers) before t_{stop}. During the time between t_{stop} and t_{start}, the corona would continue to develop, forming a corona shield around the rod tip. However, any radii with $U_c > U_{\text{stop}}$ would not develop any corona until after t_{start} and will not see any shielding effect. The relationship between U_c and rod radius indicates that smaller rod radii will be most affected by the suggested applied voltage shown in Figure 5.2.

Future research should focus on alternative waveforms for the applied voltage than the ones discussed in this thesis. By investigating the applied voltage waveform, shielding effects on time of leader initiation with respect to rod radii can be explored, and it is likely that the effect of rod radii on the time of leader initiation can be established. This relationship, in turn, can be used to quantify the strike-receptiveness of a lightning rod.

Appendix A

Non-Stationary Model Movies

"Supplemental Materials" to this thesis is a CD that contains two movies described below.

A.1 MovieLightning.avi

In the non-stationary corona and upward leader model (Chapters 3 and 4), data is best viewed through a movie to show the time dynamics of the system. This movie was represented at several specific times with Figures 4.5 to 4.8. The parameters of the model are $R_1 = 5$ cm, $R_2 = 5$ m, and $\tau = 10^{-4}$ s.

This movie can be found in *Supplemental Materials: MovieLightning.avi.*

A.2 MovieWall.avi

In the context of proposed future research, a simulation of *MovieLightning.avi* was performed with a "wall" of charge added into this system as discussed in Section 5.2. This movie was represented with Figure 5.1. The parameters of the model are $R_1 = 5$ cm, $R_2 = 2.5$ m, and $\tau = 10^{-4}$ s. The added ion density was

defined as

$$n_{\text{wall}}(r) = \begin{cases} 0 & r < 0.5 \text{ m}; \; r > 1.5 \text{ m}, \\ 1.4 \times 10^{14} \text{ m}^{-3} & 0.5 \text{ m} \leq r \leq 1.5 \text{ m}. \end{cases} \tag{A.1}$$

This movie can be found in *Supplemental Materials: MovieWall.avi*

References

Ahmad, H., and L. M. Ong (2005), An account of a modified lightning protection system for power stations, *Interna. Power Engr. Confr.*, *vol. 7*.

Aleksandrov, N. L., E. M. Bazelyan, M. M. Drabkin, J. R. B. Carpenter, and Y. P. Raizer (2002), Corona Discharge at the Tip of a Tall Object in the Electric Field of a Thundercloud, *Plasma Phys. Rep.*, *28*(11), 953–964.

Aleksandrov, N. L., E. M. Bazelyan, F. D'Alessandro, and Y. P. Raizer (2005a), Dependence of lightning rod efficacy on its geometric dimensions–a computer simulation, *J. Phys D: Appl. Phys.*, *38*(1), 1225–1238, doi:10.1088/0022-377/38/8/021.

Aleksandrov, N. L., E. M. Bazelyan, and Y. P. Raizer (2005b), The Effect of a Corona Discharge on a Lightning Attachment, *Plasma Phys. Rep.*, *31*(1), 75–91.

Aleksandrov, N. L., E. M. Bazelyan, F. D'Alessandro, and Y. P. Raizer (2006), Numerical simulations of thunderstorm-induced corona processes near lightning rods installed on grounded structures, *J. Electrostat.*, *64*(12), 802–816, doi:10.1016/j.elstat.2006.02.001.

Bazelyan, E. M. (2007), private communication.

Bazelyan, E. M., and Y. P. Raizer (1998), *Spark Discharge*, CRC Press, New York, NY.

Bazelyan, E. M., and Y. P. Raizer (2000), *Lightning Physics and Lightning Protection*, IOP, Philadelphia, PA.

Bazelyan, E. M., N. L. Aleksandrov, Y. P. Raizer, and A. M. Konchakov (2007), The effect of air density on atmospherica electric fields required for lightning initiation from a long airborne object, *Atmosph. Res.*, *86*(2), 126–138, doi:10.1016/j.atmosres.2007.04.001.

Bazelyan, E. M., Y. P. Raizer, and N. L. Aleksandrov (2008), Corona initiated from grounded objects under thunderstorm conditions and its influence on lightning attachment, *Plasma Sources Sci. Technol.*, in review.

Becerra, M., and V. Cooray (2006a), A self-consistent upward leader propagation model, *J. Phys. D: Appl. Phys.*, *39*(16), 3708–3715, doi:10.1088/0022-3727/39/16/028.

Becerra, M., and V. Cooray (2006b), Time dependent evaluation of the lightning upward connecting leader inception, *J. Phys. D: Appl. Phys.*, *39*(21), 4695–4702, doi:10.1088/0022-3727/39/21/029.

Becerra, M., V. Cooray, S. Soula, and S. Chauzy (2007), Effect of the space charge layer created by corona at ground level on the inception of upward lightning leaders from tall towers, *J. Geophys. Res. Lett.*, *112*(12), D12205, doi:10.1029/2006JD008308.

Cooray, V. (2003), *The Lightning Flash*, IEEE Power Series; 34, IEEE, London.

D'Alessandro, F. (2003a), Striking distance factors and practical lightning rod installations: a quantitative study, *J. Electrostat.*, *59*(1), 25–41, doi:10.1016/S0304-3886(03)00069-X.

D'Alessandro, F. (2007), On the optimum rod geometry for practical lightning protection systems, *J. Electrostat.*, *65*(2), 113–121, doi:10.1016/j.elstat.2006.07.011.

D'Alessandro, F., C. J. Kossmann, A. S. Gaivaoronsky, and A. G. Ovsyannikov (2003b), Experimental Study of Lightning Rods Using Long Sparks in Air, *IEEE Transactions on Dielectrics and Electrical Insulation*, *11*(4), 638–648.

Meek, J. M., and J. D. Craggs (1978), *Electrical Breakdown of Gases*, John Wiley and Sons, New York, NY.

Moore, C. B., W. Rison, J. Mathis, and G. Aulich (2000a), Lightning Rod Improvement Studies, *J. Appl. Meteor.*, *39*(5), 593–609.

Moore, C. B., G. D. Aulich, and W. Rison (2000b), Measurements of Lighting Rod Responses to Nearby Strikes, *Geophys. Res. Lett..*, *27*(10), 1487–1490.

Moore, C. B., G. D. Aulich, and W. Rison (2003), The Case for Using Blunt-Tipped Lightning Rods as Strike Receptors, *J. Appl. Meteor.*, *42*(7), 984–993.

Potter, D. (1973), *Computational Physics*, John Wiley and Sons, New York, NY.

Press, W. H., S. A. Teukolsky, W. T. Vetterling, and B. P. Flannery (1992), *Numerical Recipes in C*, 2 ed., Cambridge University, Cambridge, U. K.

Raizer, Y. P. (1991), *Gas Discharge Physics*, Springer-Verlag, New York, NY.

Rison, W. (2007), private communication.

Roth, J. R. (1995), *Industrial Plasma Engineering*, vol. 1, IoP, Philadelphia, PA.

Suli, E., and D. Mayers (2003), *An Introduction to Numerical Analysis*, Cambridge University, Cambridge, U. K.

Uman, M. A. (2001), *The Lightning Discharge*, 2001 ed., Dover, Mineola, NY.